Engineering Geology 279 (2020) 105868

Contents lists available at ScienceDirect

Engineering Geology

journal homepage: www.elsevier.com/locate/enggeo

3D numerical modelling for interpreting topographic effects in rocky hills for Seismic Microzonation: The case study of Arquata del Tronto hamlet

Ilaria Primofiore [a,*], Julie Baron [b], Peter Klin [b], Giovanna Laurenzano [b], Cristina Muraro [c], Franco Capotorti [c], Marco Amanti [c], Giovanna Vessia [a]

[a] University "G. d' Annunzio" of Chieti-Pescara, Department of Engineering and Geology, Via dei Vestini 31, 66100 Chieti, Italy
[b] National Institute of Oceanography and Applied Geophysics (INOGS), Borgo Grotta Gigante 42/C, Sgonico, 34010 Trieste, Italy
[c] Italian Institute for Environmental Protection and Research (ISPRA), Via Brancati, 48, 00144 Roma, Italy

ARTICLE INFO

Keywords:
Seismic microzonation studies
Topographic effects
3D response analysis
2016–2017 Central Italy seismic sequence
Arquata del Tronto

ABSTRACT

The 2016–2017 seismic sequence in the Central Apennines (Italy) demonstrated, once again, the relevant role of the differentiated seismic effects related to different features in complex geological contexts at a short distance (i.e. soft sediment-filled valley, hilly relieves, complex buried geometries). The heavy damages of old settlements located on the top of a rocky hill, such as Arquata del Tronto hill, raised the question on the main role of three-dimensional movements of asymmetrical isolated rocky reliefs in generating disruptions during the seismic shaking. In order to shed light on these effects, the writing authors analysed the seismic response of a digital 3D model of the Arquata del Tronto hill, that was constructed by considering the topography and the underground geological settings of the area. The seismic response was evaluated through 3D numerical simulations of seismic waves propagation with the spectral element method for the period range 0.1–1 s, that covers the typical resonance frequencies of the buildings involved in the studied case. The obtained results explain the recorded strong motion at Arquata site and are consistent with the observed heterogeneous damage distribution. This study evidences the need for accurate 3D models in the evaluation of the seismic response of ridges with topographic and geological asymmetries and demonstrates that the common usage of 2D simplified simulations to approximate the 3D seismic behaviour is not correct. Additionally, the study points out the paramount role that the characterization in engineering - geological terms plays in the numerical 3D simulation of the seismic site response. Thus, in microzoning studies, simplifications related to both dimensional and geo-litho-seismic characterizations should be avoided.

1. Introduction

From August 2016 to January 2017, a seismic sequence struck the Central Apennines (Italy), involving tens of municipalities and producing heavy damages, as well as about three hundred casualties. The first shock on 24th August 2016, at 1:36 UTC, occurred near Amatrice and Accumoli with Mw 6.0 and hypocentral depth of 8 km and was followed by an Mw 5.4 event at 02:33 UTC close to Norcia (reference website: itaca.mi.ingv.it). They caused extensive and irregularly distributed damage over the area (Galli et al., 2016). Subsequent shocks (on 26th October, M_w 5.4 at 17:10 and M_w 5.9, at 19:18 UTC, on 30th October, Mw 6.5 at 5:40 UTC, and finally on 18th January 2017 four shocks with Mw ranging from 5.0 to 5.5) aggravated the level of damage (Graziani et al., 2019; Lanzo et al., 2019). The damage spatial pattern indicates that strong local modifications of earthquake ground motion (i.e. site effects) took place in the area (Sextos et al., 2018) due to stratigraphic and topographic effects. As a matter of fact, in the aftermath of the first mainshock of the 2016–2017 sequence, the macro-seismic surveys reported an EMS intensity 8–9 at Arquata del Tronto old town located along the rocky ridge. On the other hand, 7 EMS intensity was reported at the Borgo hamlet located in the alluvial valley at the foothill (Graziani et al., 2019; Lanzo et al., 2019). This case study represents a typical example of complex seismic site effects in Central Apennines (Amanti et al., 2020).

* Corresponding author.
E-mail addresses: ilaria.primofiore@alumni.unich.it (I. Primofiore), jbaron@inogs.it (J. Baron), pklin@inogs.it (P. Klin), glaurenzano@inogs.it (G. Laurenzano), cristina.muraro@isprambiente.it (C. Muraro), franco.capotorti@isprambiente.it (F. Capotorti), marco.amanti@isprambiente.it (M. Amanti), g.vessia@unich.it (G. Vessia).

https://doi.org/10.1016/j.enggeo.2020.105868
Received 21 April 2020; Received in revised form 12 October 2020; Accepted 13 October 2020
Available online 17 October 2020

The study presented hereinafter intends to shed light on the occurrence of the so-called "atypical topographic effects" in the case of asymmetric rocky ridges. Typical topographic effect defines the response of homogeneous rock hills when the morphology is the main factor that contributes to the ground motion amplification. Instead, the atypical topographic effect is referred to several factors (that are structural and geological heterogeneities) concurring to the definition of the site response (Burjanek et al., 2014). This latter contribution may imply higher amplification values, a broadening of the amplification frequency range and a kinematic pattern in the horizontal plane - a parasitic twisting motion- which can severely increase the damage level on buildings. To this aim, we adopted a well-established 3D numerical modelling method for seismic waves propagation, that is the Spectral Element Method (SEM), to investigate the site response of Arquata del Tronto hill and its surroundings. The open-source SPECFEM3D-Cartesian code (Peter et al., 2011) was used to perform numerical simulations.

A fundamental step for addressing 3D numerical simulations consists of setting-up an accurate 3D model of the subsoil geological structure using a computer-aided 3D geological modeller. This step was accomplished through the commercial software GeoModeller (https://www.intrepid-geophysics.com/product/geomodeller, last access: 7th January 2020), using geological and geomorphological data that were collected in the framework of Seismic Microzonation studies of the Arquata del Tronto municipality (ISPRA, 2017).

In the following, Section 2 is devoted to the description of some other authors relevant studies in seismic topographic effects; Section 3 introduces the study area, summarises the observed damage pattern at Arquata del Tronto and Borgo hamlets and describes the construction of the 3D digital geological model of the study area. Section 4 illustrates the methods we employed for the 2D and 3D numerical simulations. Finally, we illustrate the results and an explanation of the observed differentiated damage pattern in Section 5.

2. State of the art in the study of topographic effects

The term "topographic effect" defines seismic motion modifications that occur as the topographic surface reflects, diffracts, scatters or refocuses the incident seismic waves. Numerous cases of seismic damage variability in areas with notable relief (Davis and West, 1973; Çelebi, 1991; Vessia et al., 2013, 2016) suggests that topographic effects may have a significant impact on ground motion in the frequency range, where most buildings are vulnerable. While researchers have so far conducted quite extensive theoretical and experimental investigations of topographic site effects (see Paolucci (2002) and Massa et al. (2014), among others, for a rather exhaustive overview of the topic) the development of a robust quantification approach is still at its early days. Some authors (Massa et al., 2014; Barani et al., 2014) made a distinction between typical and atypical effects. This latter distinction has been systematically studied by field observations and numerical simulations during the recent NERA European project (Burjanek et al., 2014). As a synthesis of a large number of analysed case studies, the "topographic effects" turn out to be a complex combination of two contributions: the topographic features and the local sub-surface conditions (mechanical and geometrical characters) of soils and rocks. Researchers found that all but A Eurocode 8 soil classes suffer motion amplification at site-dependent frequencies and along with selected directions. Pischiutta et al. (2018) performed a systematic analysis using stations of the Italian seismic network to derive an indication about the occurrence of topographic amplification. They did not obtain any systematic relations between seismological evidence and morphology, concluding that other features in the subsoil should have a prevailing role in producing directional effects, such as large-scale open cracks (Marzorati et al. 2011; Moore et al. 2011; Burjanek et al., 2014) and/or microcracks in fractured rocks (Pischiutta et al., 2013, 2015a, 2015b).

2.1. Experimental studies

The topographic effects have been extensively investigated through field measurements and numerical simulations. From experimental studies, the polarization in the slope seismic response was at first highlighted by Spudich et al. (1996), who found that seismic motion on a ridgetop is polarized perpendicularly to its elongation as an effect of wave scattering. This effect was confirmed by many other authors (e.g. Burjanek et al., 2014; Del Gaudio and Wasowski, 2011). This topic has been studied both in soil and rocky slopes through ambient noise HVSR, standard spectral ratio SSR and arrays of strong earthquake seismographs. Results pointed out the occurrence of stronger spectral amplifications along the maximum slope direction in soil slopes (Del Gaudio and Wasowski, 2011). In rocky slopes, using several different experimental and numerical techniques, Burjanek et al. (2014) found the maximum ground motion amplification was oriented along the steepest slope. This latter effect is often combined with the heterogeneity of the fractured slope surface into a complex behaviour that cannot be thoroughly understood if numerical simulation models do not consider them all (Kazemnia Kakhki et al., 2020). Using observational data from a dense array of strong earthquake seismographs deployed along the Lengzhuguan slope (China), He et al. (2020) studied its seismic response to the 2008 Wenchuan earthquake. They highlighted that the seismic ground motion on the ridgetop was polarized perpendicularly to its elongation with an amplification factor higher than 10 in the frequency band ranging between 1.5 and 2.5 Hz, where the rocky slope was covered by a loose deposit layer of about 30 m depth. Sepúlveda et al. (2005) highlighted that during the 1994 Northridge earthquake (6.7 M_w) significant topographic amplifications have been experienced along rocky ridges in California and measured by local accelerometric stations: the peak accelerations measured at the crests were more than 3 times larger than the ones measured at the foothill. Finally, Zhang et al. (2018) measured the seismic response of the Xishan Park ridge under the 2008 Wenchuan earthquake using the SSR technique: the field results showed that topography and local presence of soft materials on the surface significantly increases the ground motion. The maximum amplification factor, as large as 4, was observed at the hilltop within the frequency range of 1–10 Hz.

2.2. Numerical simulations

Concerning the numerical simulation experiences performed in the literature on seismic slope response, the first 2D ones were performed in the '80s on simplified ridge models, with a constant velocity through the section (see Géli et al., 1988 and the references therein). These studies explained slope amplification in terms of wave scattering by the convex shape of topography and the amplified resonance frequency depending on the hill dimension and its velocity. The growing number of available data has recently permitted several back-analyses of 2D and 3D ridge models with numerical methods. Ding et al. (2020) studied the effects of surficial soil properties (Vs, thickness and material) on topographic amplification, based on a 2D slope model with horizontally stratified soil layers, with nonlinear elastoplastic behaviour. The results confirmed that the extent of the topographic effect gradually increases with Vs values decreasing. Gischig et al. (2015) dealt with the seismic response of unstable deep rocky slopes. With a series of 2D numerical models, they explored the role of seismic amplification to increase the amplitude of the co-seismic slope deformation, considering Vs, topography and fractures. 2D results show that 3D modelling is needed to understand the co-seismic slope deformations. Furthermore, Paolucci (2002) studying four isolated, irregular and densely inhabited relieves in Italy evidenced that 2D numerical simulations underestimate the amplification factors for all the topographic categories listed by the Eurocode 8. This is true in the cases of narrow and large isolated cliffs, ridges with crest significantly shorter than the base and the average slope angles both lower and higher than 30°. Additionally, Paolucci evidenced strong 3D effects that

cannot be approximated by 2D seismic response analyses. A method for predicting topographic amplification was presented by Maufroy et al. (2015), who uses the curvature of the surface, defined as the second spatial derivative of the elevation map, as a proxy for the topographic amplification. This method was used with promising results to predict the observed damages at Amatrice, after the 24th August 2016 earthquake (Maufroy et al., 2018). Lately, Luo et al. (2020) investigated the topographic effects at the rocky Mt. Dong and Weigan hill in Sichuan Province (China) using monitoring data and 2D and 3D numerical modelling performed through Udec 2D and 3D codes. They measured amplifications as large as 5–6 times the input motion that was predicted by 3D numerical models only if they reconstructed the complex combination of the topographic and subsurface geological setting of the area. In general, numerical simulations of slope seismic response underestimate the measured amplification factors (Massa et al., 2014; Lovati et al., 2011; Géli et al., 1988; Spudich et al., 1996; Paolucci et al., 1999). This discrepancy has been attributed to a common oversimplification of the geometries, i.e. 2D instead of 3D ridge models, that demonstrated to be unable to reproduce, in several cases, the complexity of the seismic wavefield modifications (Massa et al., 2014). Hence, in the present work, both 2D and 3D numerical analyses have been performed at Arquata del Tronto steep rocky ridge, based on a detailed reconstruction of geo-lithological and seismic subsoil model, to understand its complex seismic response.

3. The case study of Arquata del Tronto

Arquata del Tronto (42.7725 N, 13.2963 E) is an Italian municipality set in the Marche region. It is located in the Central Apennine belt, at the base of the South-East flank of Vettore Mount. While the Old Town is located on a small rocky hill, the municipality has an area of 92 km^2, consisting of 13 hamlets (Fig. 1). Among these, the hamlet of Borgo has been recently urbanized, at less than 1 km from the Old Town, in the valley beneath it. In this work, the following acronyms were used for the sites of major interest (Fig. 2): site STA, for the Old Town of Arquata del Tronto; site STB, for the hamlet of Borgo; site STC is located in the Western part of the Old Town, at the base of a medieval Castle, almost 200 m uphill from the Old Town.

3.1. Recent seismicity and differentiated damages occurred

The town of Arquata del Tronto, being in the centre of the Apennine chain, suffers from the influence of numerous nearby faults, even a few kilometres away. The Database of Italian Seismogenic Sources (DISS Working Group, 2018) shows many faults in the surroundings of Arquata del Tronto: they were, and potentially will be, sources of destructive earthquakes for the municipality. The proximity and the number of active faults determine a very high seismic risk. In Table 1, historical earthquakes that shook Arquata del Tronto over time with a macroseismic intensity on Mercalli-Cancani-Sieberg scale (MCS) higher than 6 are listed (https://emidius.mi.ingv.it/CPTI15-DBMI15/). Thus, this territory has been mostly affected by seismic events generated in the same areas as the 2016–2017 seismic sequence.

.

Graziani et al. (2019) performed a throughout and exhaustive study of the damages caused by the seven events whose magnitude was larger than 5.4 (the first occurred on 24th August 2016, Mw 6.0, with the main event felt on 30th October 2016, M_w 6.5).

The authors described the damages through the European Macroseismic Scale intensity I_{EMS} (Grünthal, 1998), reporting the spatial

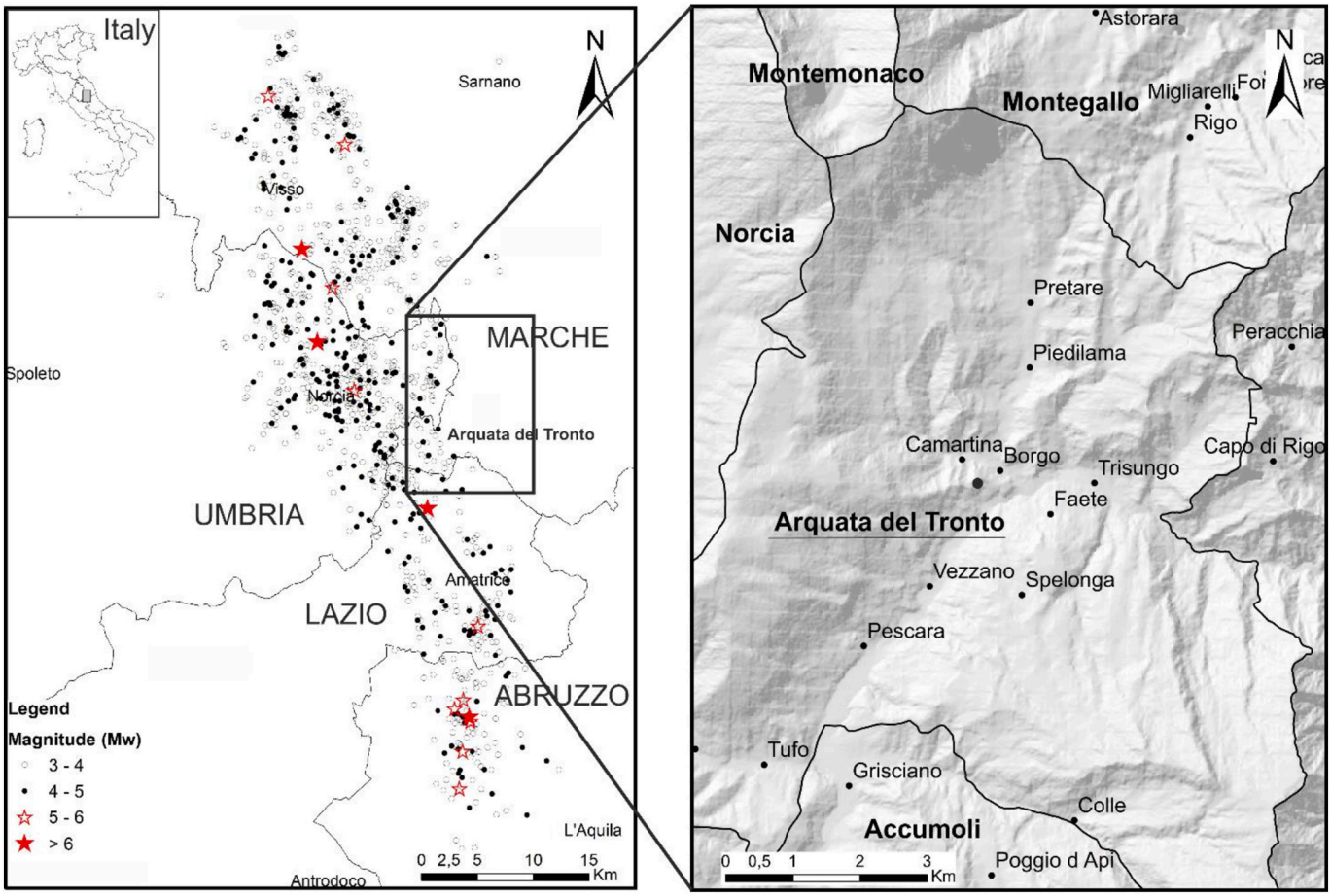

Fig. 1. Epicentre location map of several events generated by the 2016–2017 Central Italy seismic sequence.

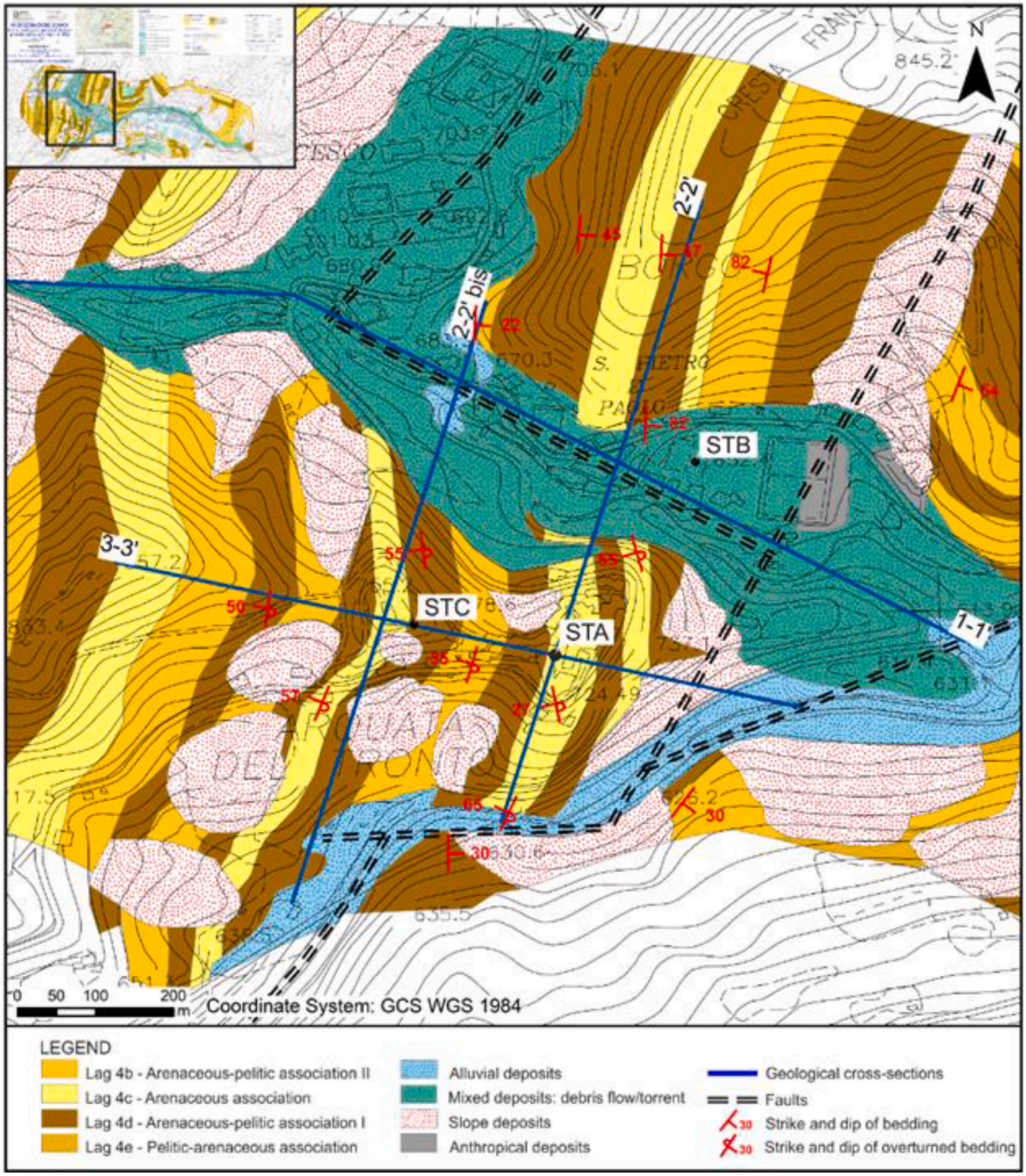

Fig. 2. Simplified extract of the geological and geomorphological map used for the level 3 Seismic Microzonation studies of the Macroarea 1 Arquata del Tronto and Montegallo (AP), with section names and acronyms used for the sites of major interest.

distribution of the damage magnitude for different vulnerability classes (VC) of buildings. VC decreases from A that means high vulnerability (simple stone masonry with irregular texture and a generally bad state of preservation) to D meaning low vulnerability (reinforced concrete structures with anti-seismic design and a good state of preservation). At site STA, the damage was equally distributed among buildings of vulnerability classes A and B, whereas class B suffered major damage at site STB.

After the first shock, at site STA, most buildings (72%) were affected by structural damage and few buildings underwent total destruction (14%). This behaviour has been recognized on both VC A and B, especially located on the steep and external portion of the hill. The behaviour

Table 1
Seismic events that caused macroseismic effects higher than 6 MCS in Arquata del Tronto.

Intensity to Arquata del Tronto	Date	Epicentre	Epicentral intensity	Mw
9	1703-01-14	Valnerina	11	6.9
7–8	1730-05-12	Valnerina	9	6.0
7	1916-07-04	Monti Sibillini	6–7	4.8
6–7	1972-11-26	South Marche	8	5.5
6–7	1950-09-05	Gran Sasso	8	5.7

of vulnerability class A corresponded to 9 I_{EMS}, while class B experienced 8 I_{EMS}.

At site STB, slight and medium damage was observed in buildings of vulnerability class A and B, and the damage scenario is as high as I_{EMS}. In the aftermath of the last earthquake (30th October), 9–10 I_{EMS} was assessed at site STA, while at site STB the damage reached 8–9 I_{EMS}. The differences in the accumulated damage pattern at Arquata del Tronto and Borgo hamlets are caught by Laurenzano et al. (2019), Lanzo et al. (2019) and Giallini et al. (2020) studies. They suggested that 3D topographic amplification conditioned the local site effects. Accordingly, the writing authors reconstructed 2D and 3D numerical models of the area, to investigate possible kinetic and inertial effects induced by the seismic wave propagation.

3.2. Geological and seismotectonic features

The study area is located on the outer edge of the Central Apennines at the foot of the Olevano-Antrodoco-Sibillini Mountains thrust, in the Western outcropping area of the Messinian turbidite deposits of the Laga Formation. According to the Seismic Microzonation studies of the Macroarea 1, Arquata del Tronto and Montegallo (map at 1:5.000 scale by ISPRA (2017)), the siliciclastic deposits occurring at Arquata del Tronto correspond to the Campotosto member of the Laga Formation (LAG_4). The member is subdivided into many units characterized by different arenite/pelite (A/P) ratio. In the analysed area, four lithofacies associations of this member crop out: the arenaceous association (LAG_{4c}), the arenaceous-pelitic association I (LAG_{4d}), the arenaceous-pelitic association II (LAG_{4b}) and the pelitic-arenaceous association (LAG_{4e}). The subsoil geology of Arquata del Tronto consists of a repeated alternation of the previous four lithofacies. Other details can be found in Appendix A. A detailed geological and geomorphological map of the area was drawn for the level 3 Seismic Microzonation studies of the Macroarea 1 Arquata del Tronto and Montegallo (AP) (ISPRA, 2017) and it can be downloaded for free (http://www.halleyegov.it/c044006/hh/index.php). A simplified and cut out version of the map is shown in Fig. 2, together with the related geological cross-sections (Figs. 3, 4, 5) investigated in this study.

The beds are oriented toward the West with high angle slope. From ISPRA surveys, they were classified as a reverse side according to the hypothesis that they are part of a large overturned anticline fold, developed in the hanging-wall of a thrust. This interpretation also derives from the work of Centamore et al. (1991). The original geological cross-sections have been slightly modified by the ISPRA geologists who processed them to be give more details for 3D modelling purpose. The main change from the original version concerns the concavity of the beds of the fold located below the old town of Arquata del Tronto, to follow-up on overturned fold hypothesis. Accordingly, a high degree of fracturing on the surface was detected, believed to be related to successively normal faulting.

The local bedrock is mostly covered by continental deposits, consisting of calcareous detritus mixed to arenaceous boulders, in a sandy silt matrix, alluvial and alluvial terraces deposits, of variable thickness, based on the genesis of the deposit and the morphology of the accumulation area.

3.3. Geophysical and lithotechnical characterization

At the end of September 2016, ten temporary seismological stations were installed in the municipality of Arquata del Tronto to evaluate the site response (Laurenzano et al., 2019). Two out of them have been deployed in the area under study: MZ85 station (at STB site) and MZ80 station (at STC site). At STA site, there are no continuous recordings from seismological stations. From their analyses, Laurenzano et al. (2019) inferred the site response at STB and STC through both the Generalized Inversion Technique (GIT) applied to S-wave amplitude spectra of earthquake recordings and the Horizontal to Vertical Spectral Ratio of seismic noise (HVSR). The results, in terms of spectral amplification, evidenced that site STB presents a single-peaked response at 4.5 Hz (0.22 s), on the seismologic station MZ85, for the horizontal components of the ground motion, whereas at site STC (seismologic station MZ80) the response exceeds the value 2 over a broad range of values, from 1.5 to 4.5 Hz (0.22–0.67 s). Moreover, many geophysical investigations were carried out during Seismic Microzonation studies (ISPRA, 2017). At the site STC, from the background noise recording (with Horizontal to Vertical Spectral Ratio analysis), amplified frequencies of about 3 Hz (0.33 s) were found. At site STB, amplification peaks at 4.5 Hz (0. 22 s) can be definitively recognized. At site STA, investigation results captured frequencies between 2 and 3 Hz (0.3–0.5 s). From the information retrieved, we decided to group the four lithofacies of the Laga Formation into two, according to their geophysical and mechanical properties, as shown in Table 2. As a result, we use 2 litho-technical units, one predominantly arenaceous (i.e. LAG_{4c} + LAG_{4d}), the other mainly pelitic (i.e. LAG_{4e} + LAG_{4b}), in addition to the Quaternary deposits, belonging to a single litho-technical unit, which onlaps over all the alternations of the various lithofacies of the LAG_4 member. In the seismic response analyses, a shallow layer of fracturing and alteration was also considered.

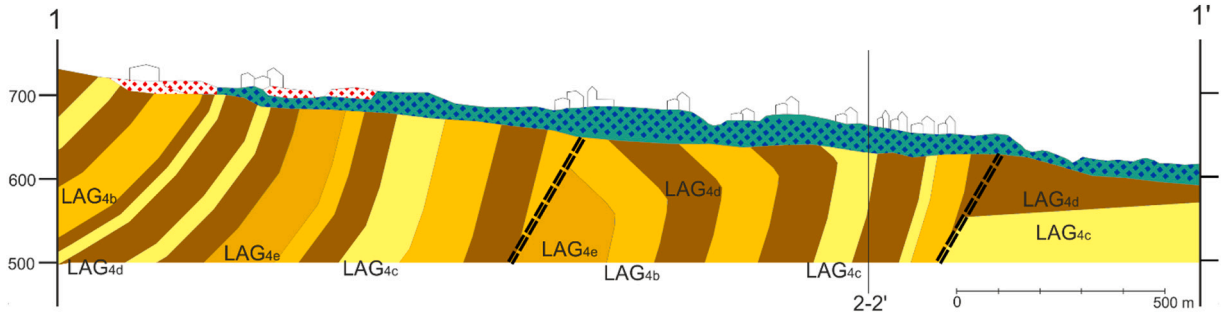

Fig. 3. Geological section 1–1′ from Fig. 2.

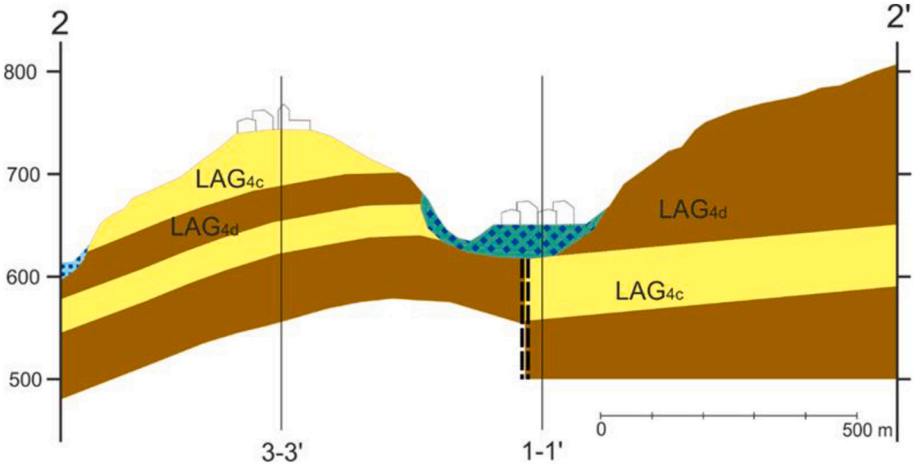

Fig. 4. Geological section 2–2′ from Fig. 2.

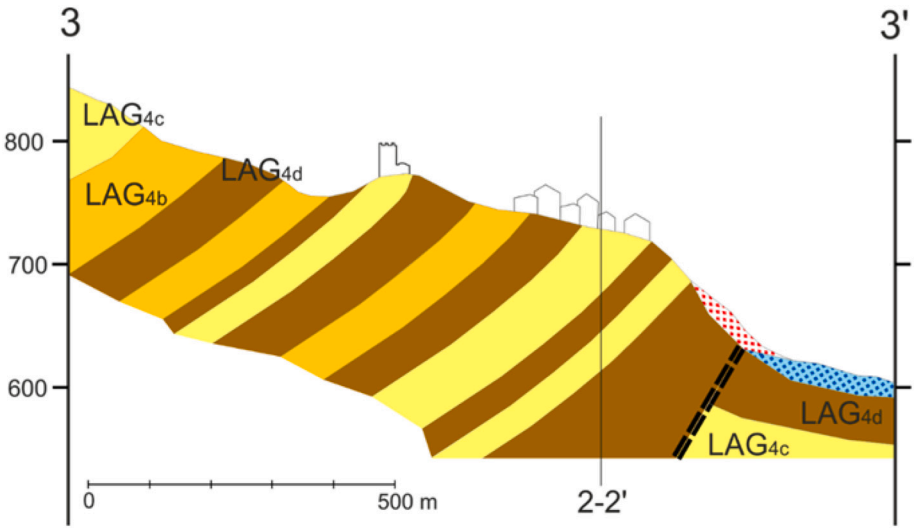

Fig. 5. Geological section 3–3′ from Fig. 2.

Table 2
Material properties used in both 2D and 3D numerical simulation models.

Layers	Vs (m/s)	Vp (m/s)	Density ρ (kg/m^3)	Curves G/G$_0$ e D/D$_0$	Qμ	Q$_K$
Alluvial deposits	450	1100	1800	Rollins et alii	45	160
Alteration layer	700	1700	2000	Linear D = 1%	70	245
Pelitic association	900	2250	2100	Linear D = 0.5%	90	315
Arenaceous (bedrock) association	1000	2500	2200	Linear D = 0.5%	100	350

The material properties were obtained from previous studies (Puzzilli et al., 2019; Ciancimino et al., 2019) and from investigations conducted during the data acquisition survey (investigations and results from Level 3 microzoning activities at Arquata del Tronto municipality can be found on http://www.halleyegov.it/c044006/hh/index.php, last access October 2020). We define the characteristics of the arenaceous association from a Down Hole (DH) investigation, carried out at site STA. Based on other DH investigations, the parameters for the pelitic association have also been defined. Vs =700 m/s was assigned to the alteration layer and Vs = 450 m/s to the deposits based on Multichannel Analysis of Surface Waves (MASW) tests. MASW results were preferred to DH investigations, as the former is indicative of average properties along a transept while the latter represent punctual measurements.

3.4. 3D digital geologic model

Since 3D subsoil geological models represent the basis for the execution of 3D numerical simulations, a digital geological 3D model of the study area has been built by integrating the collected surface and subsurface data with a computer-aided process. To this aim, we adopted GeoModeller (Calcagno et al., 2008; Guillen et al., 2004), a commercial software which allows building complex and implicit 3D geological models directly from geological observations. GeoModeller was recently used to build up a structural and geophysical 3D digital model of the Po plain sector involved in the 2012 seismic sequence with the purpose to perform physics-based numerical simulations of earthquake ground motion (Klin et al., 2019). More details about GeoModeller can be found in Appendix B.

The 3D geological model that was set up for Arquata del Tronto covers a square area of 2 km × 2 km down to a depth of 1 km (Table 3) and is centred at STA site.

The model was built by importing into GeoModeller the following data:

Table 3
Dimensions and spatial position of the 3D model. Coordinates are given in WGS 1984 UTM zone 33 N reference system.

Min lon (km)	Max lon (km)	Min lat (km)	Max lat (km)	Min alt (m)	Max alt (m)
359,606	361,596	4,736,026	4,738,016	200	1200

- A high-resolution Digital Terrain Model at a grid size of 10 m of the area (Fig. 6a) (Tarquini et al., 2007);
- An excerpt of the geological-geomorphological map for the third level Seismic Microzonation studies of the Macro Area 1 Arquata del Tronto and Montegallo (AP) (ISPRA, 2017), which reports the main geological units outcropping in the area, as well as the tectonic structures (Fig. 2);
- Three geological sections (Figs. 3, 4, 5): 1–1′ crossing site STB and Camartina localities in almost EW direction, 3–3′ almost parallel to 1–1′ and crossing both STA and STC sites, 2–2′ transversal to 3–3′ section and crossing both STA and STB sites.

To constrain the geometry of the different lithofacies, we manually digitized, on the geological-geomorphological map and along the cross-sections, the interfaces between them as well as the fault traces, attributing to the latter their extension, their relationship with the geological succession and their relationship with other faults. In GeoModeller, the building of the 3D model includes several steps, with a progressive integration of the available data. At each step, we perform a computation of the implicit surfaces of the lithofacies boundaries and check the partial result before adding new elements. The final 3D geological model obtained by GeoModeller is displayed in Fig. 6b. The volumes corresponding to the different geophysical bodies are shown.

4. Numerical modelling of seismic wave propagation

4.1. 2D numerical simulation

To confirm the expected different seismic responses at different morpho-litho-seismic site conditions, STA and STB sites have been studied employing 2D numerical simulations and compared to the 3D analyses.

4.1.1. 2D numerical simulation settings

2D numerical analyses have been performed through the commercial code LSR2D by STACEC (www.stacec.com) based on the finite element method. Its theoretical references are illustrated in Appendix C. Fig. 7a shows the section 2–2′, where the 2D equivalent linear numerical analyses have been accomplished. The section has been divided into 37,244 triangular 3 m wide elements (Fig. 7b).

4.1.2. Input motion for 2D simulation

The input motion, given at the bottom of the model domain, is a set of seven accelerograms that are compatible (within the range 0.1–1.1 s) to the target acceleration spectrum provided by the Italian Building Code (NTC18), assuming a horizontal acceleration with a probability of exceedance of 10% in 50 years, referring to stiff soils ($Vs_{eq} > 800$ m/s; cat. A) according to the Reference Italian Seismic Hazard Map (GdL MPS, 2004 approved by the Decree of the Prime Minister OPCM n.3519/2006. The seven accelerograms and related spectra (Fig. 8) were selected, for the municipality of Arquata del Tronto, by Luzi et al. (2019) during the Central Italy third level Microzonation study (ISPRA, 2017). All the records are related to normal fault source mechanism and reference site A*.

4.2. 3D numerical modelling

The continuous development of advanced numerical methods and computational power facilities have made technically feasible the simulation of seismic wave propagation in 3D heterogeneous media and the computation of realistic seismic ground motion records at the surface in a frequency range of interest in seismic design applications. As a consequence, it has arisen the interest for the integration of such 3D physics-based numerical simulations in seismic hazard analyses to further improve seismic ground motion prediction. 3D physically based numerical simulations can provide a detailed and accurate characterization of the seismic ground motion, allowing the exploration of its spatial heterogeneity. Therefore, they appear as a powerful and efficient tool for an accurate estimation of local seismic amplification effects that are useful in understanding the differentiated damages caused by strong earthquakes.

4.2.1. 3D response functions

The seismic site effect is usually regarded as a time-invariant linear system, therefore we evaluated the site effects over the Arquata del Tronto hill and its surroundings in terms of 3D impulse response functions, as described in Paolucci et al. (1999). The 3D response function consists of a 3 × 3 matrix with components $h_{ij}(\boldsymbol{x},t)$. The time series $h_{ij}(\boldsymbol{x},t)$ describes the i^{th} spatial component of the seismic time series that would be observed at the site $\boldsymbol{x}$ when the area is invested by a vertically incident impulsive plane wave polarized in the j^{th} direction with unitary amplitude. We can express the modified ground motion $\boldsymbol{y}(\boldsymbol{x},t) = [y_1(\boldsymbol{x},t), y_2(\boldsymbol{x},t), y_3(\boldsymbol{x},t)]$ at the site $\boldsymbol{x}$ for any vertically incident seismic input $\boldsymbol{u}(t) = [u_1(t), u_2(t), u_3(t)]$ as

$$y_i(\boldsymbol{x},t) = \Sigma_j\, h_{ij}(\boldsymbol{x},t) * u_j(t) \quad (1)$$

where * denotes convolution in time. The expression is usually evaluated in the frequency domain, substituting the convolution with multiplication by the convolution theorem.

$$Y_i(\boldsymbol{x},f) = \Sigma_j\, H_{ij}(\boldsymbol{x},f)\, U_j(f) \quad (2)$$

where uppercase letters denote the Fourier transforms of the corresponding time-series denoted by lowercase letters.

In the present work, we evaluated the theoretical response functions $h_{ij}(\boldsymbol{x},t)$ on the topographic surface of a given 3D structural model from the time domain numerical solutions of the visco-elastodynamic equation for three cases of a vertically incident plane wave: 1) shear wave polarized in the East-West direction, 2) shear wave polarized in the North-South direction, 3) compressional wave (Up-Down polarization).

4.2.2. Spectral elements method

Physics-based numerical modelling of seismic wave propagation in 3D heterogeneous visco-elastic media at frequencies of engineering interest (i.e. of the order of 10 Hz) represents a demanding computational task. Typically, the computational cost requires the usage of parallel algorithms and high-performance computing (HPC) resources. Several accurate and computationally efficient numerical methods for modelling the earthquake ground motion in 3D heterogeneous media has been developed so far (e.g. Moczo et al., 2014). The method we adopted hereinafter is called the Spectral Element Method (SEM), that was introduced in the study of acoustic and elastic waves by Seriani and Priolo (1994). SEM is a high order numerical method that combines the geometrical flexibility of Finite Elements Methods (FEM) with the accuracy of the spectral methods. Like FEM, SEM is based on the solution of the variational formulation of the equation of motion in non-overlapping spatial subdomains (elements), in which we subdivide the investigated volume. Unlike FEM, SEM represents the wavefield in each element in terms of spectral polynomial bases of a high order, with a significant gain of accuracy. SEM has proved to be effective in modelling earthquake ground motion (e.g. Komatitsch and Vilotte, 1998; Peter et al., 2011), and thanks to the geometrical flexibility it resulted particularly suitable for cases where an irregular topographic surface is involved (e.g. Lee et al., 2009). To apply the SEM method to the case

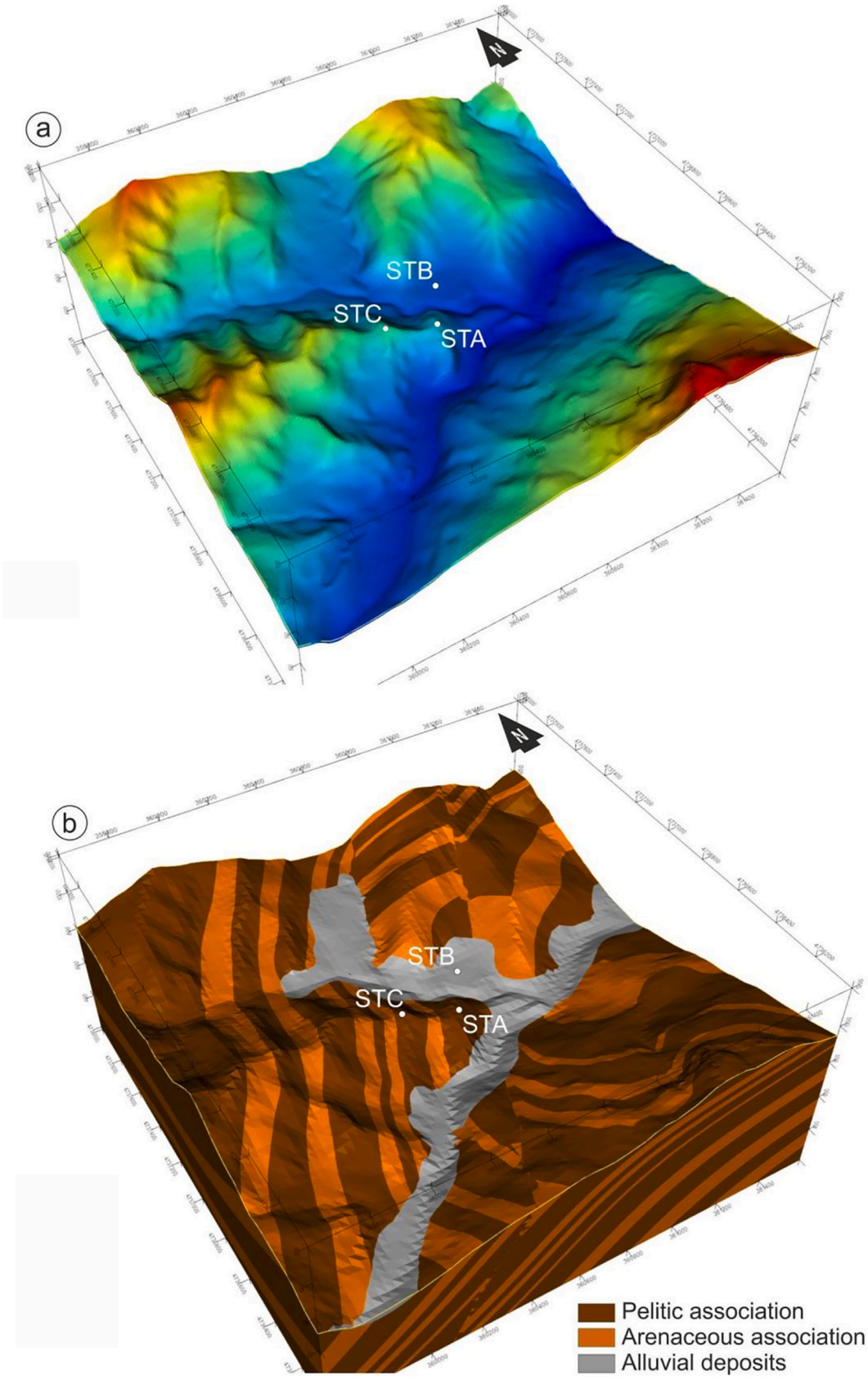

Fig. 6. a) Digital Elevation Model; b) 3D model computed by GeoModeller. The model is built according to a cartesian reference frame, where x-axis points East and y-axis points North. The spatial coordinates of the x and y axes are referred to the kilometric reference system WGS 84 UTM zone 33 N. The units of measurement of the z-axis refer to the meters above sea level.

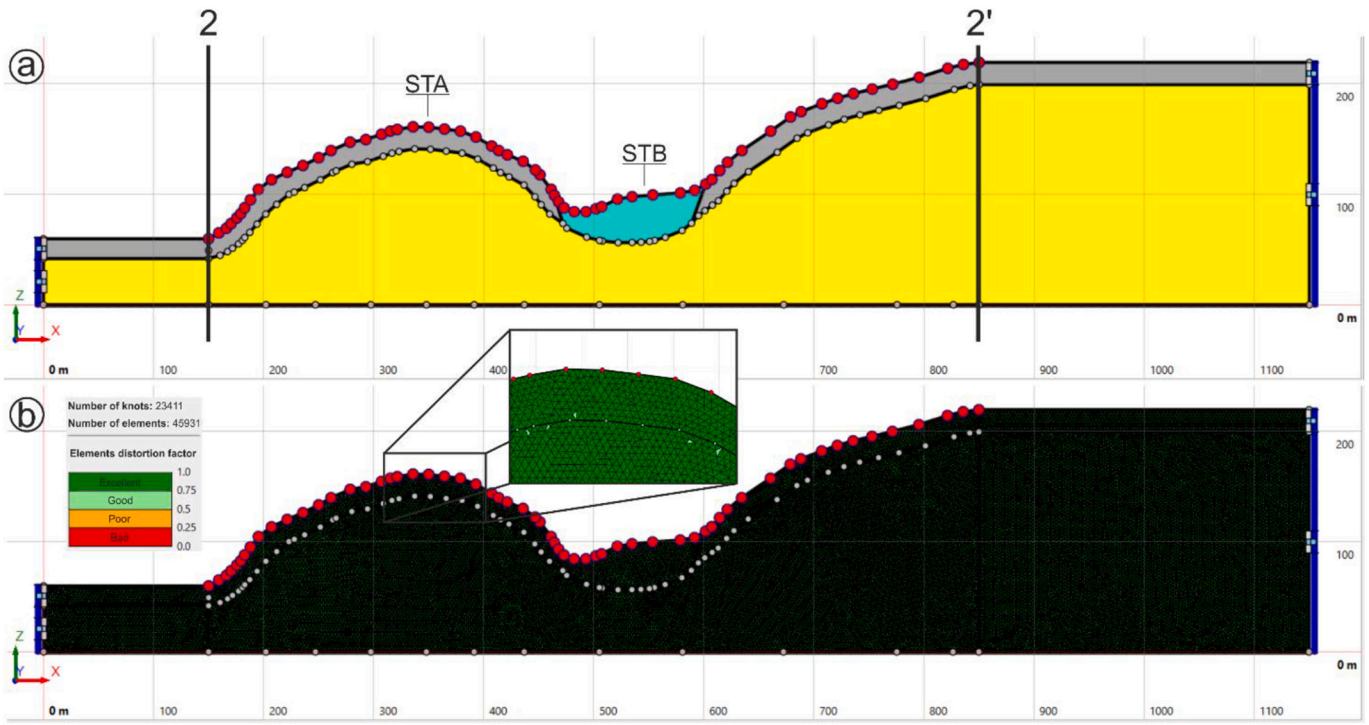

Fig. 7. (a) The spatial domain for 2D numerical simulations with the LSR2D code (Stacec s.r.l.) across section 2–2′. Arquata del Tronto and Borgo hamlets. Legend: yellow = pelitic association; light blue = alluvial deposits; grey = alteration layer. The red points on the surface are the measuring points of the seismic signal. (b) Mesh and boundary conditions of the 2D model. (For interpretation of the references to colour in this figure legend, the reader is referred to the web version of this article.)

study discussed in this work, we adopted the open-source software SPECFEM3D Cartesian (https://geodynamics.org/cig/software/specfem3d/, last access 28th June 2019), which consists of implementing the SEM based on the discretization of the spatial domain in hexahedral elements and the wavefield expansion in Legendre polynomials (Komatitsch and Tromp, 1999). The code accounts for the intrinsic attenuation properties of the viscoelastic medium by a series of Zener standard linear solids (Komatitsch and Tromp, 2002) and avoids the boundary reflection artefacts thanks to the usage of Perfectly Matched Layers (Xie et al., 2014).

SPECFEM3D is suitable to run on HPC machines, where we can shorten its execution time by distributing the computational tasks over a high number of processors. The computations related to the present work were performed using the HPC resources available at CINECA through the Italian SuperComputing Resource Allocation service - ISCRA (http://www.hpc.cineca.it/services/iscra).

4.2.3. 3D numerical simulation settings

The most demanding step in the preparation of a numerical simulation of seismic waves propagation with SPECFEM3D is the definition of the computational spatial domain, that consists in an unstructured hexahedral mesh according to the geometry of the 3D geomodel. The numerical modelling in the present work is based on a mesh that was generated through the SPECFEM3D internal meshing machine with the following specifications:

- Horizontal base: a square area at −500 m a.s.l. with 3 km long sides aligned with the cardinal points and centred at STA site;
- Top surface geometry: 10 m-resolution TINITALY DEM (Tarquini et al., 2007);
- Element size: ranging from 25 m at the topographic surface to 50 m at the flat bottom surface with doubling layer at sea level (Fig. 9).

Given the element size at the topographic surface, we neglected the presence of the thin deposit layer except for the limited area around site STB (Fig. 9), where a thicker layer of deposits was detected (ISPRA, 2017).

The resulting mesh consists of 518,400 elements: each of them was characterized by the mechanical properties of the structural unit occupying its position in the 3D geologic model. Considering the values of the mechanical properties (Table 2), the dimensions of the elements imply a time step as short as 0.0005 s to satisfy the stability criterion of the time marching step implemented in the SPECFEM3D solver and that accurate solutions of seismic waves up to the frequency of 10 Hz can be obtained. On the other hand, the finiteness of the overall size of the considered spatial domain undermines the meaningfulness of the modelling results for frequencies below 1 Hz.

The polarized vertically incident plane waves, that were required for the evaluation of the response functions, were generated with a horizontal carpet of point sources at -400 m a.s.l, with an explosive mechanism for the vertically polarized plane wave and West-East or North-South oriented double couple mechanism for the two independent cases of horizontally polarized plane waves, respectively.

The SPECFEM3D solver was configured to output 8 s long three-component time series evaluated in a dense regular grid of points on the topographic surface, on three cross-sections 2–2′, 2-2′ bis and 3–3′ (Fig. 2) and in three points STA, STB and STC. STB and STC, corresponding to the location of the temporary stations MZ85 and MZ80, were used to compare the numerical results with site observations in the present paper.

The computational cost of each run amounted around 900 CPU hours distributed among 225 processing units of the Marconi supercomputer at CINECA.

5. Results and discussion

In the following, we first evidence the variability of the site effects in the studied area as they result from 3D numerical simulations by

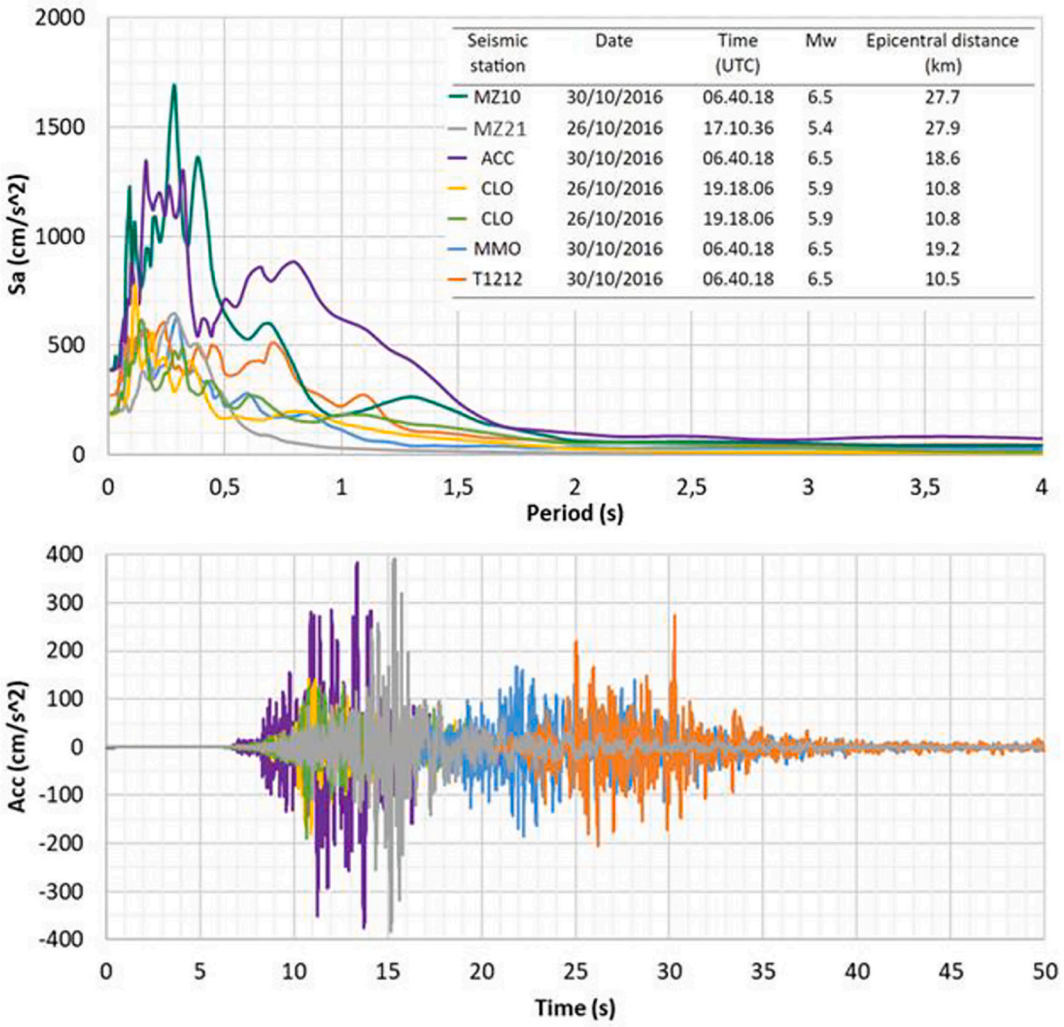

Fig. 8. Time histories and response spectra of seven accelerograms used as input motion for numerical simulations (Luzi et al., 2019).

plotting the horizontal transfer functions along some lines across the area under investigation (Subsection 5.1). Next, we attempt validation of the 3D simulations at the two sites STA and STB, using horizontal to vertical spectral ratios from earthquake recordings described in Laurenzano et al. (2019), (Subsection 5.2). Finally, we point out the differences between the 3D and 2D simulations in terms of the response spectra for specific seismic input at sites STA and STB and in terms of amplification functions and Housner's amplification factors evaluated along the line 2–2′ (Subsections 5.3 and 5.4).

5.1. 3D transfer functions

In Fig. 10, we plot the Fourier amplitude spectra of the NS and EW component of the numerical response obtained from the 3D model for a vertically incident shear plane wave polarized in the NS and EW direction, respectively, along the lines 2–2′, 2-2′ bis and 3–3′ (see map in Fig. 2). In the bottom panels, we show a vertical cross-section along the same lines to correlate the changes in the spectra with the topographic profile and structural features.

Sections 2–2′ and 2-2′ bis are almost N-S oriented and therefore the NS and EW components correspond approximately to the response of in-plane (P-SV) and out-of-plane (SH) motions, respectively, whereas section 3–3′ runs nearly in the E-W direction and the interpretation of the components in terms of in-plane and out-of-plane motion is exchanged there.

Fig. 10 points out a prominent spatial variability in the frequency-dependent site effects predicted with the numerical simulation. The largest amplification values are observed on the N-S component, which is perpendicular to the main axis of the relief (the ridge is approximately E-W oriented). For both the components, we can observe that the largest amplification is concentrated in correspondence with the top of the relief with multiple peaks corresponding to the modes of vibration of the hill. Moving away from the top, we observe an alternation of amplification and de-amplification along the slope due to constructive and destructive interferences of the seismic waves inside the hill structure, a typical topographic effect already evidenced by Komatitsch and Vilotte (1998). The base of the relief is characterized by low values and, in some cases, de-amplification effects occur.

5.2. H/V spectral ratios from earthquake recordings

A large number of seismic recordings was collected at sites STB and STC during the 2018 seismic sequence (Laurenzano et al., 2019). However, because of survey logistics (the same instrument was installed at the two sites during different time intervals), no simultaneous recordings at the two stations exist, and a validation attempt for 3D numerical simulations in terms of the relative amplification of the same component between sites STB and STC was not feasible. We therefore resorted to the description of the site effect in terms of the horizontal-to-vertical (H/V) spectral ratio of earthquake recordings (Lermo and

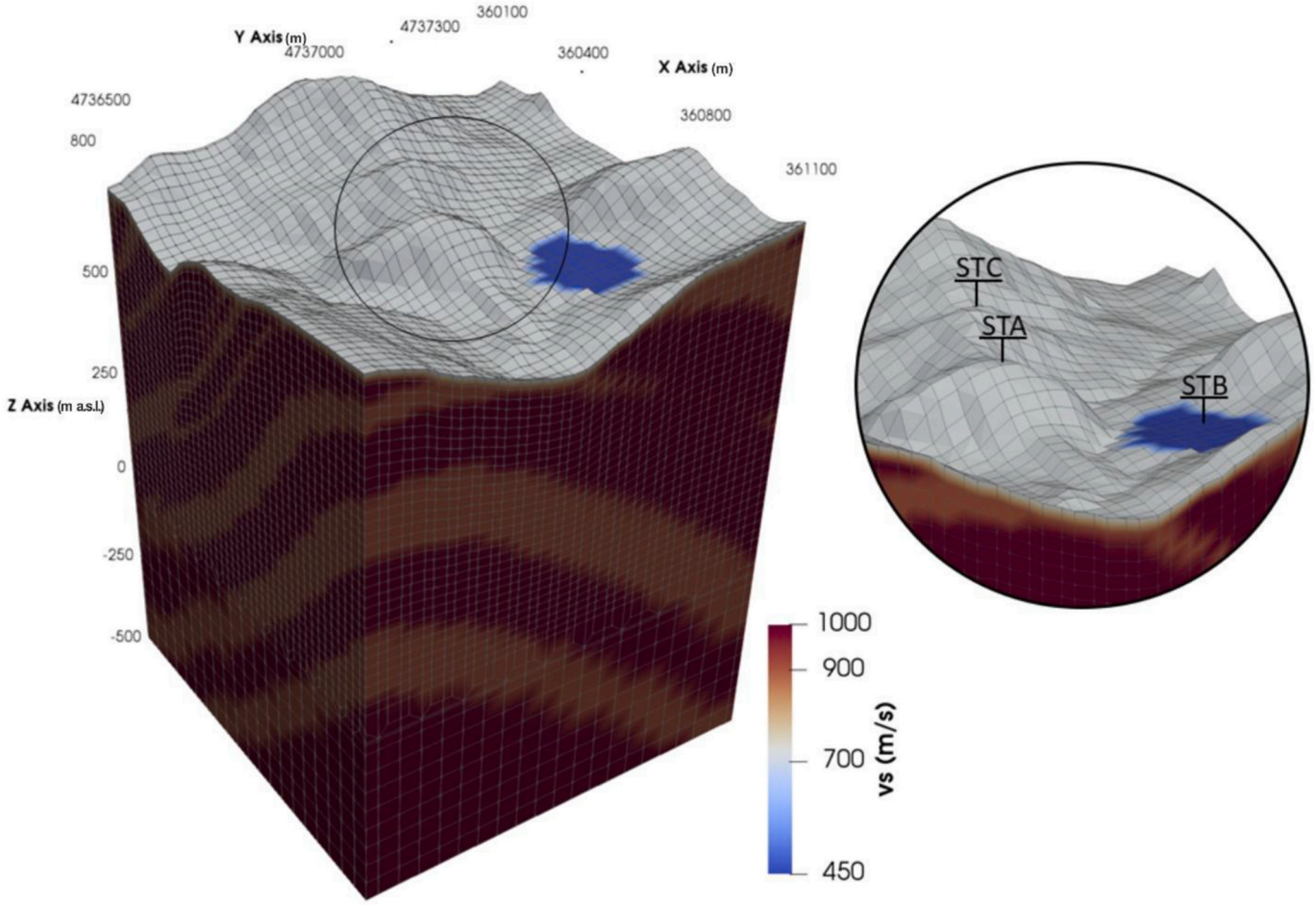

Fig. 9. SPECFEM3D mesh for the 3D geophysical and lithotechnical model centred at the study area. The spatial coordinates of the x and y axes are referred to the kilometric reference system WGS 84 UTM zone 33 N. The units of measurement of the z-axis refer to the meters above sea level.

Chavez-Garcia, 1993). We simulated a set of earthquake recordings at stations STB and STC by means of convolution of the numerical 3D response functions at STB and STC with a set of almost two hundred seismic inputs. As seismic inputs, we considered the recordings collected during the same survey by Laurenzano et al. (2019) at the station MZ75 located on geological bedrock at about 12 km far from hamlet Uscerno.

In Fig. 11, we display the mean H/V spectral ratios for experimental and simulated data (black and blue lines respectively). The shadow area represents the standard error and the two dashed lines represent the mean for the two horizontal components considered separately.

For site STC, the curves obtained from the simulated ground motion are characterized by an alternation of peaks (at about 2, 3 5 and 9 Hz) and notches between them, with a low-moderate level of amplification (below 3). The curves obtained from the observed ground motion exhibit a similar pattern but with higher values for frequencies below about 4.5 Hz and lower values for higher frequencies. The underestimation of the H/V in the low-frequency part of the spectrum may be due to the limited extension of the spatial domain that we considered in the simulations. In fact, the Arquata hill is part of a larger structure, which is truncated and smoothed out in our 3D model and whose contribution to the site response results neglected. On the other hand, the polarization effects evidenced by the difference between the separate horizontal components are rather consistent in the simulated and observed data.

For site STB, located in the valley, the simulated data predicts a mean peak value of about 2 at about 5 Hz instead of the value 3 at about 4.5 Hz given by observed data, but these differences are in the order of magnitude of the standard error.

Even though these comparisons do not provide a strict validation for the adopted 3D model, they suggest a substantial correctness in the adopted parametrization.

5.3. Site-specific response spectra

The response spectra for 5% damping have been estimated from 2D and 3D simulations, given a seismic input compatible with the Uniform Hazard Spectrum, calculated for a 10% exceedance probability level in 50 years (return period of 475 years), as defined by the Italian seismic code (NTC18). See Section 4.1.2 for all the details about the characteristics of the seismic input. In particular, we obtained the 3D response spectra by the convolution of the seismic input with the 3D model response functions (Eq. (1)).

Fig. 12 shows the Site-Specific Response Spectra obtained from 3D simulations at the three selected sites (blue lines). At sites STA and STB, they are compared with those obtained by 2D simulations (green lines). For sites STB and STC we also plot (red dotted lines) the Site-Specific Response Spectra obtained from the convolution of the seismic input with the experimental site amplification curve calculated for a rock reference site by the site-response analysis of Laurenzano et al. (2019). The spectra of the Italian building code NTC18 for the ground types and topography category appropriate for the three sites (i.e. A and T3 category for sites STA and STC, STB and T1 for site STB) are also reported (dashed orange lines). We can observe that, for all the cases, the NTC18 spectra underestimate the amplification recorded in the seismological stations, and therefore underestimate the numerical response spectra, for periods higher than 1 s, for sites STA and STC, and higher than 0.5 s for site STB. The downfall of the response spectra can be

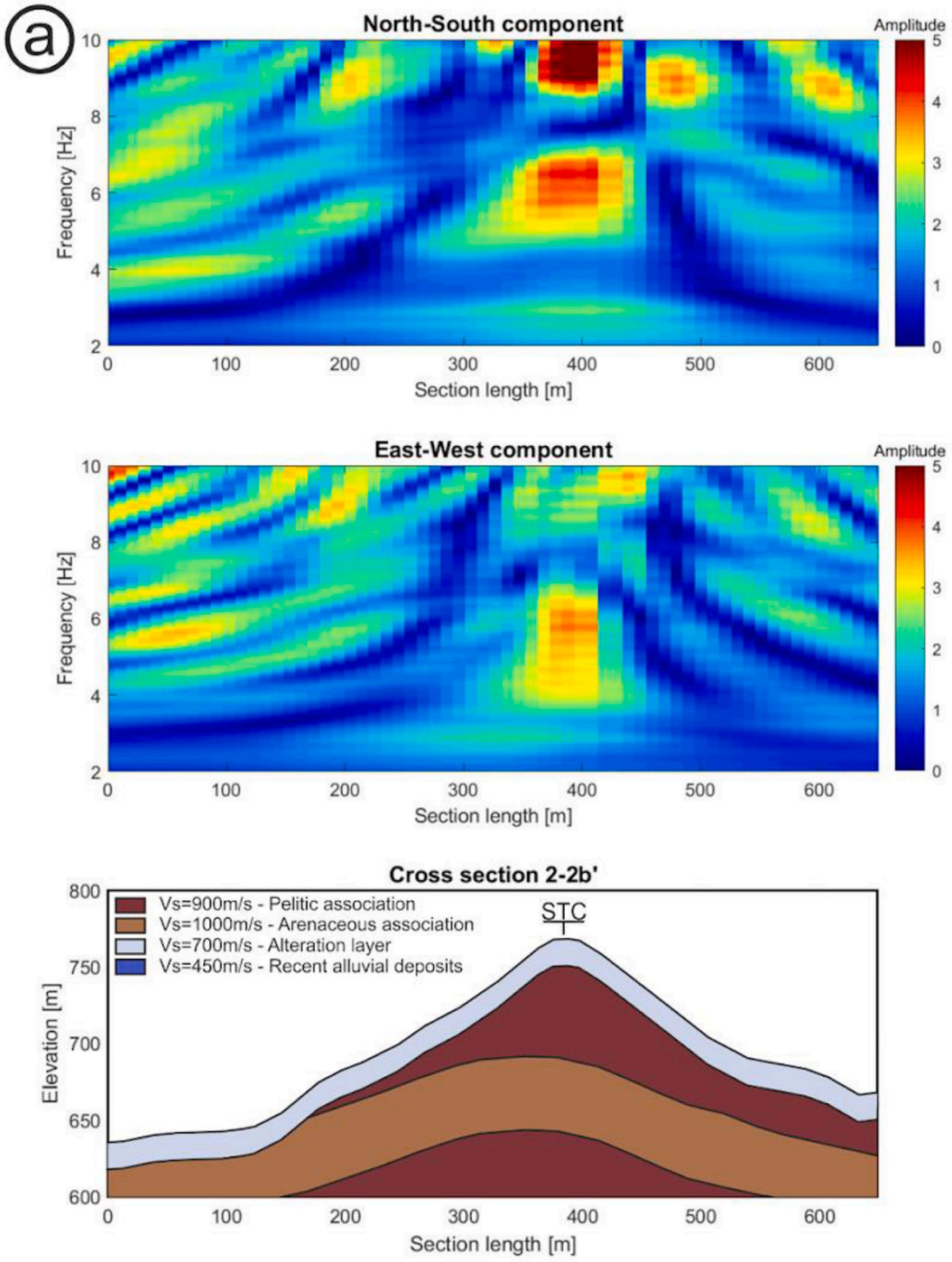

Fig. 10. Transfer functions obtained from 3D simulations on three studied sections. (a) cross-section 2–2′ bis; (b) cross-section 3–3′; (c) cross-section 2–2′.

probably attributed to the limited dimension of the spatial domain considered in, both 2D and 3D simulations. On the other hand, in the period band 0.1–1 s, the NTC18 curves underestimate both the numerical and the experimental spectra up to a factor of 2. Differences between 2D and 3D curves are not that relevant in shape, but the mean 3D response spectra are always greater than the 2D ones.

At site STA (Fig. 12a), the response spectra from 2D and 3D simulations exhibit similar behaviour, with two peaks around 0.15 s and 0.25 s, although 3D predicts higher values than 2D. These amplifications are almost uniform over the upper part of the hill for the 2D simulations, as can be seen from the little dispersion of the response spectra in light green. On the contrary, the dispersion of the response spectra amplifications is quite large from the 3D simulations, with a range of about 0.4 g along the spectral ordinate.

The simulated response spectra at site STB fit quite well with the experimental one (Fig. 12b): the predominant peak at 0.2–0.25 s is predicted by both 2D and 3D simulation, thought slightly shifted toward higher periods.

At site STC, (Fig. 12c) the comparison between 3D and experimental spectra shows differences, especially regarding the shape of the curves. Amplitudes instead are quite similar, approximately for all periods but especially below 0.3 s. This site appears to be the most amplified among

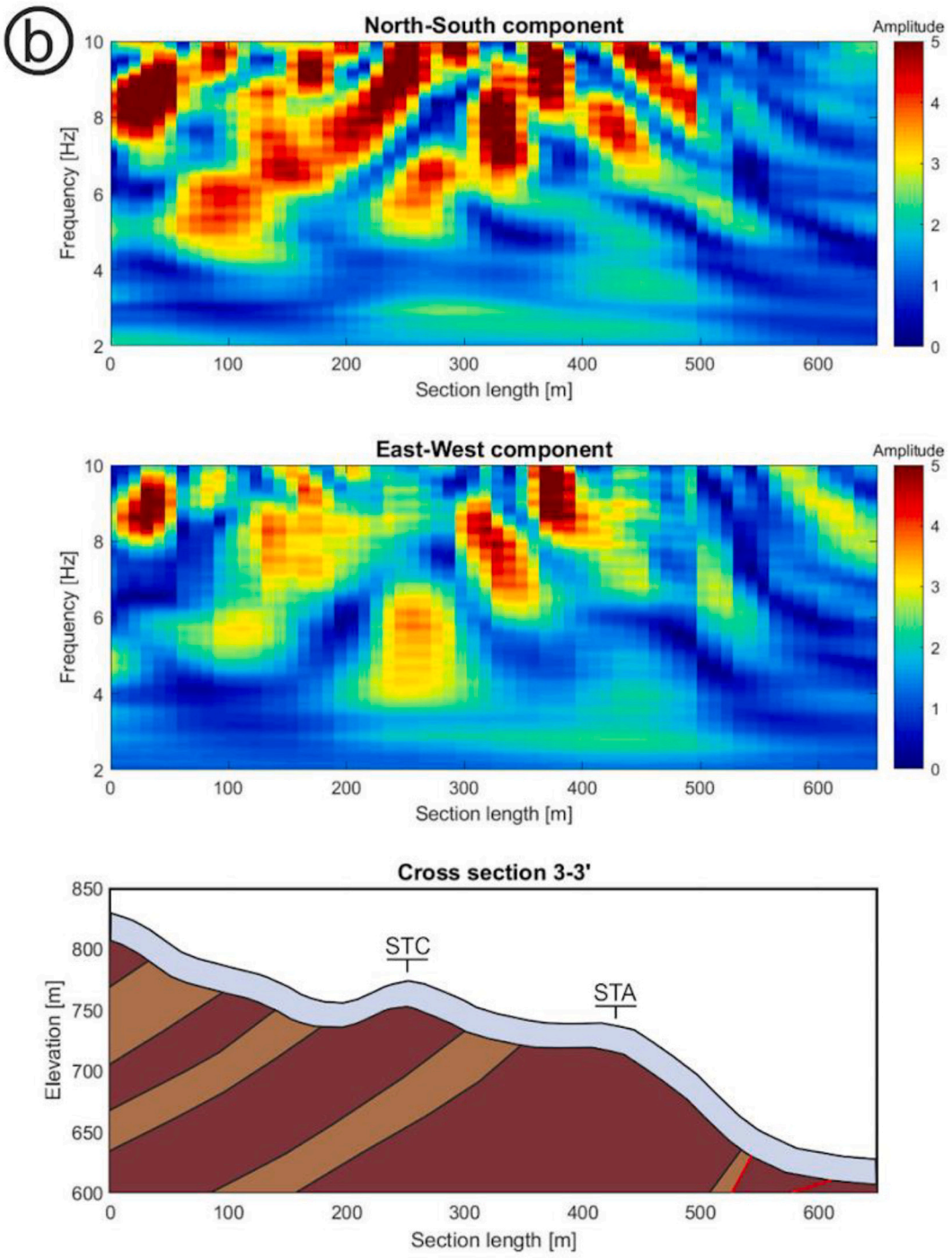

Fig. 10. (*continued*).

the three analysed, with the maximum values of about 1.5 g, compared to NTC18 curve for which a spectral acceleration of 0.7 g is expected on the plateau.

5.4. Amplification functions and Housner's amplification factor

To have a better insight on the differences between the 2D and 3D simulations we compared the two in terms of the amplification function and the Housner's amplification factor along the line 2–2′ which includes the sites STA and STB. We define the amplification function as the ratio between the response spectra of the simulated ground motion and the response spectra of the corresponding seismic input. On the other hand, we define Housner's amplification factors as the ratio of the Housner's Spectral Intensity (SI) of the simulated ground motion and the corresponding seismic input:

$$FA_H = \frac{\int_{T_1}^{T_2} PSV_{out} dT}{\int_{T_1}^{T_2} PSV_{in} dT} \quad (3)$$

where PSV_{out} is the output pseudo-velocity spectrum at a location; PSV_{in} is the input pseudo-velocity spectrum at the same location of the PSV_{out}; T_1 and T_2 represent the extremes of two-period ranges of calculation. We considered two-period ranges: a "short" period range with extremes $T_1 = 0.1$ s and $T_2 = 0.5$ s and a "long" period range with extremes $T_1 = 0.5$ s

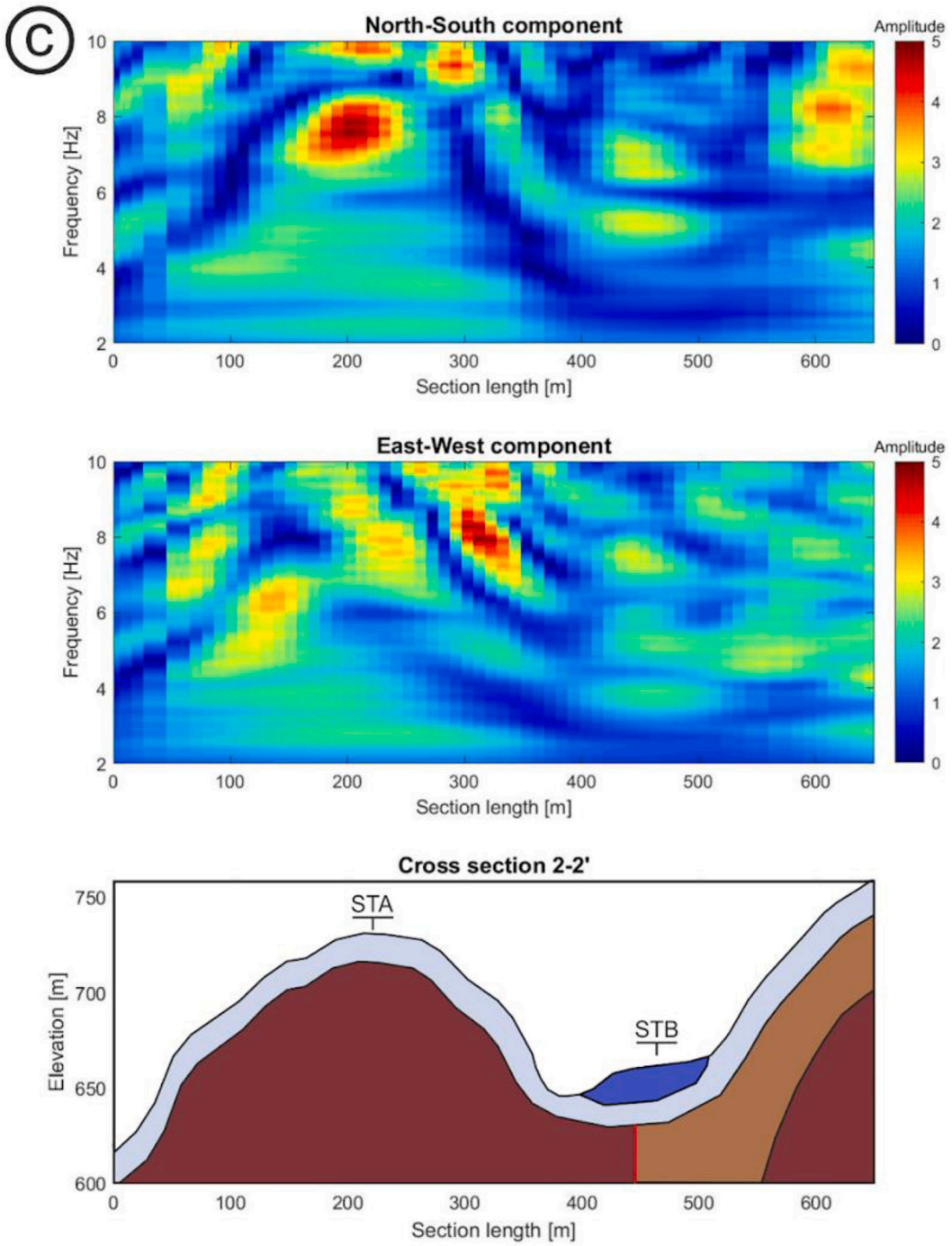

Fig. 10. (*continued*).

and $T_2 = 1.0$ s.

In Fig. 13 (I and II panel) we compare the amplification functions (the ratio between output and input acceleration spectral responses) obtained from 2D and 3D simulations along section 2–2′ for the SH component of ground motion. The 2D model predicts the largest amplification in correspondence of the sediment valley (where site STB is located) with the amplification level larger than 2 between 4 and 6 Hz (T = 0.17–0.25 s) whereas at site STA the predicted amplification is lower and involves a frequency range restricted to between 2.5 and 3.5 Hz (T = 0.29–0.4 s). On the contrary, the 3D model predicts a lower amplification at site STB while at site STA and in its surroundings corresponding to the topographic relief it predicts large amplification values over the whole considered frequency range. We can conclude that in comparison to the 3D simulations the 2D simulations underestimate the topographic effects and overestimates the valley effects. These results are summarized in the curve of the Housner's amplification factors calculated from 2D and 3D simulations along the section (Fig. 13, III panel) in two-period ranges: FA_1 = [0.1–0.5] s (continuous line), FA_2 = [0.5–1] s (dashed line).

It appears that in the studied case, the amplification levels evaluated with the 3D simulation are consistent with the observed damage distribution while the 2D simulation contradicts it.

Fig. 14 illustrates the values of the Housner amplification factors evaluated in the two-period ranges from 3D simulations over the whole studied area. The short-period band (FA1) presents local amplification patches as the one on the top of the hill (site STC), the Arquata del

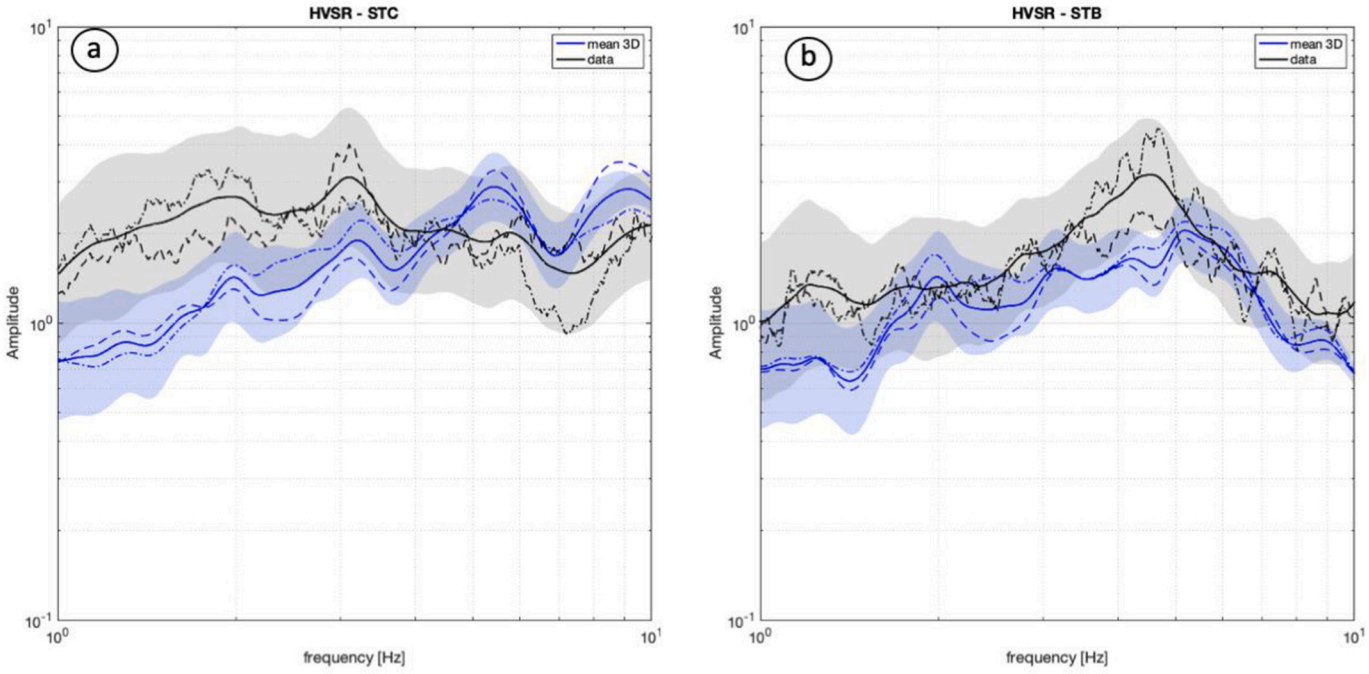

Fig. 11. H/V spectral ratios from earthquake recordings calculated by 3D simulations and experimentally by earthquake recordings by Laurenzano et al. (2019) at two sites of Arquata del Tronto municipality: (a)Site STC – MZ80 (the Castle over the hill); (b) Site STB – MZ85 (Borgo hamlet, on a sediment-filled basin). Dash-dotted and dashed lines refer to EW and NS, respectively.

Tronto centre (site STA), the surrounding ridges and the Borgo alluvial basin. On the other hand, the long-period band (FA2) is characterized by an amplification next to 2 at STA and its neighbourhood, but it is negligible in the basin where Borgo (site STB) is located.

To visualize the dependence of the response of the 3D model to the polarization of the solicitation, we plot in Fig. 15 the peak values of the two horizontal components of the time-domain response function corresponding to a soliciting impulse of the same direction.

Thanks to the nearly East-West orientation of the Arquata del Tronto ridge, we don't need to rotate the NS and EW component of the response function to investigate the response in the ridge-parallel and ridge-perpendicular components. From Fig. 15 it appears quite clearly how the ridge-perpendicular component (the NS one) exhibits the largest peak values along the ridgetop. This behaviour could be reasonably associated with the amplification of the vibration of the ridge in the component perpendicular to its elongation observed by He et al. (2020) and Pischiutta et al., 2010. On the other hand, we can observe that the peak values of the other component (the EW one) present local maxima on the secondary NS oriented crests that descend from the main ridge in correspondence of the outcrop of the arenaceous lithofacies. The points on the ridgetop located on arenaceous lithofacies are therefore subjected to the amplification in both the horizontal components, which could explain the heavy damaging observed there.

An interesting aspect of the distribution of the ground motion throughout the surface of the 3D model emerged by representing the resultant vector of the horizontal components of the instantaneous acceleration vectors. Fig. 16 shows a snapshot of the horizontal accelerations obtained with the convolution of the 3D response functions with the signal input corresponding to the recording of the Mw = 5.4 foreshock of the day 30th October 2016 in the station T1212 (Avendita) at an epicentral distance of about 15 km. For each point, the direction of the resultant is represented as a vector. The snapshot is extracted from the arrival of the S waves train and the vector length is proportional to the acceleration amplitude. It can be observed that along the secondary ridge (about NS oriented) on which Arquata del Tronto centre is located, the vectors are not aligned along with preferential directions but describe a rotary motion. The fact that two neighbouring points have two different vector directions creates a twisting effect in the ground, which likely could be transferred to the structures above. This torsional component of the ground motion, due to the ground motion incoherence of the asymmetric ridge (Anagnostopoulos et al., 2015), can generate an accidental eccentricity that adversely affects most of the building owing generalized severe damage or collapse.

6. Conclusions

The complete disruption suffered by Arquata del Tronto town, Central Italy, set on a rocky asymmetric ridge made up of the Laga Formation and, on the contrary, lighter damage pattern observed at Borgo hamlet, set on soft to stiff alluvial valley deeper than 30 m, induced the writing authors to investigate the complex seismic behaviour of the Arquata del Tronto rocky ridge by not only 2D but also 3D numerical simulations of physics-based modelling of seismic wave propagation. Comparing the numerical simulation results in terms of acceleration response spectra and amplification functions, the following conclusions can be pointed out:

- At Borgo site, 2D simulations overestimated the level of seismic amplification compared to 3D simulations even though at the same resonant frequencies. The differences in predicted amplification amplitudes can be reasonably referred to the simplification of the geometry in 2D models and the trapping of the energy in a smaller area rather than the 3D actual volume;
- At Arquata del Tronto old town, 2D simulations predicted amplifications that are lower than those at Borgo site. Instead, the 3D simulations predicted large amplification over the ridgetop and a complex pattern of amplification and de-amplification along the flanks of the asymmetric hill. The amplification along the ridgetop is especially effective in the NS component which is perpendicular to the elongation of the ridge. Nonetheless, amplifications along the secondary oriented crests have been observed (EW direction) where arenaceous lithofacies outcrop. The points on the ridgetop located on

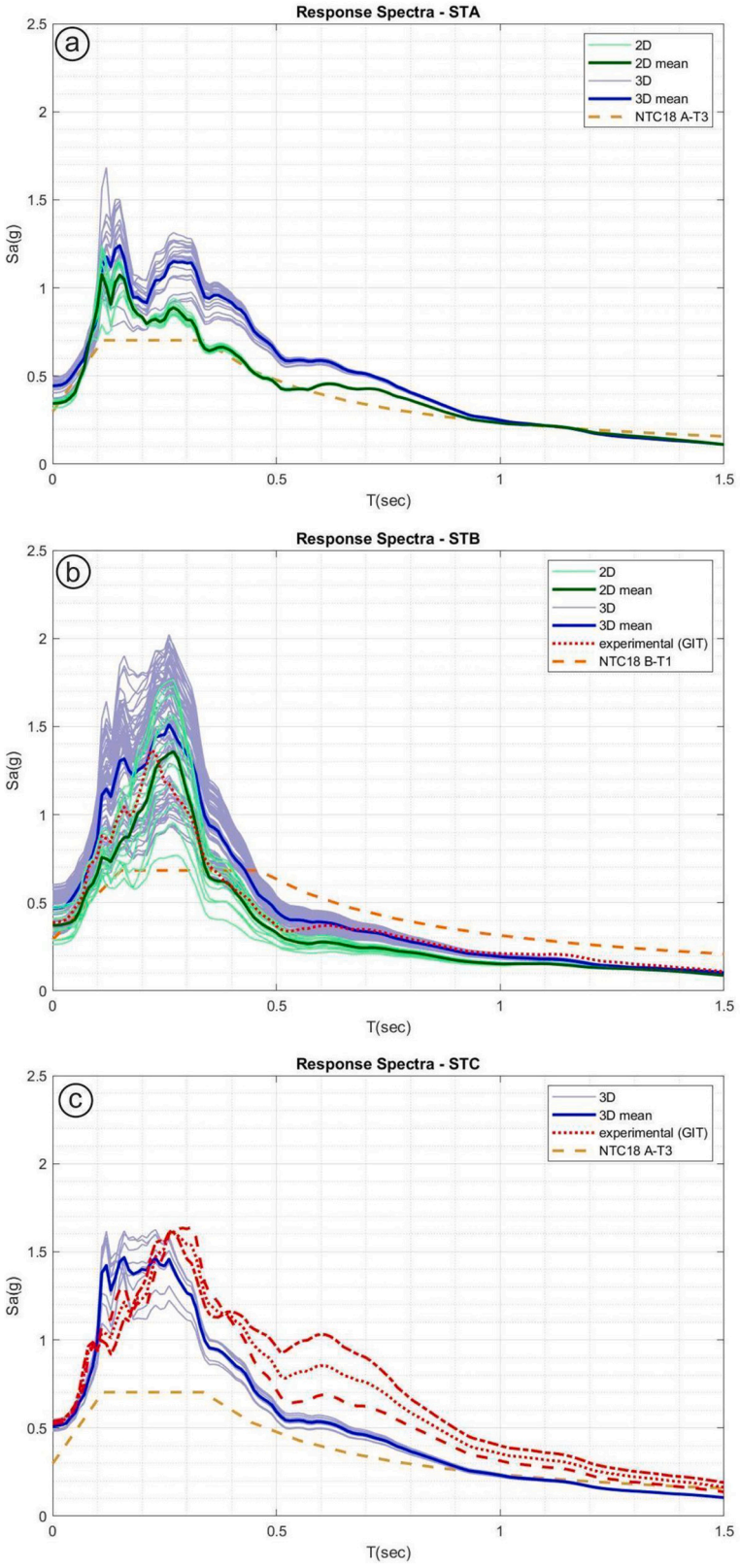

Fig. 12. Acceleration response spectra calculated by 2D and 3D simulations at the three sites of Arquata del Tronto municipality: (a) Site STA (Arquata del Tronto Old Town, on the ridge); (b) Site STB – MZ85 (Borgo hamlet, on a sediment-filled basin); (c) Site STC – MZ80 (the Castle over the hill), red dash-dotted and dashed lines refer to GIT EW and NS component, respectively. (For interpretation of the references to colour in this figure legend, the reader is referred to the web version of this article.)

arenaceous lithofacies are therefore subjected to the amplification in both the horizontal components, which could explain the heavy damaging observed there,

- At the Castle site, the 3D acceleration response spectra correctly reproduced the main features of the strong motion event recorded there on 30 Oct 2016.
- The study of kinetics at Arquata del Tronto ridge highlighted that twisting particle movements can be traced in the horizontal plane,

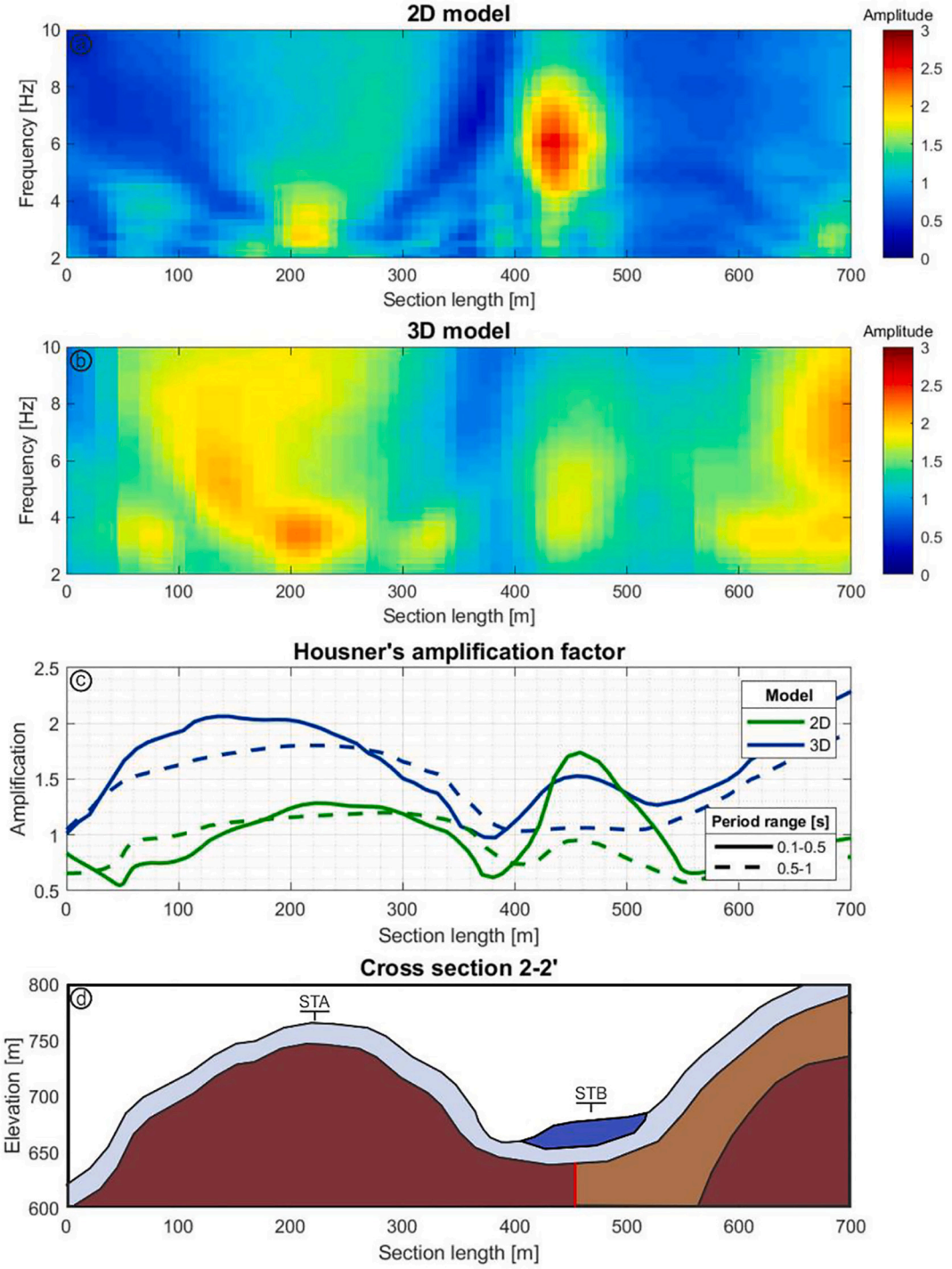

Fig. 13. Amplification functions calculated by 2D (a) and 3D (b) simulations along the cross-section 2–2′. Housner's amplification factors are calculated (c) along section 2–2′ by both 2D and 3D simulations. Blue curves: 3D model; green curves: 2D model. Full line: 0.1–0.5 s; dashed line: 0.5–1 s. Cross-section to which the Housner's amplification factors refer is represented in (d). (For interpretation of the references to colour in this figure legend, the reader is referred to the web version of this article.)

that likely caused additional solicitations responsible for the large disruption suffered by Arquata del Tronto ridge site.

The present study demonstrated the need for 3D simulations instead of 2D ones, commonly used even when the plane symmetry conditions related to both the topography and the geology are broken (SM Working Group, 2015). Additionally, 3D simulation results are influenced by the accurateness of the geological and geophysical 3D digital model reconstruction which allowed us to predict a plausible map of the ground motion amplification effects in a restricted area around Arquata del Tronto hamlet, for the frequency band 1–10 Hz.

The map results are compliant with the observed damage distribution and evidence the role of the combination of topographic and stratigraphic effects for the seismic hazard in morphologically and geologically complex areas, like those in the Central Apennines. For this reason, the authors suggest using 3D simulations at third level

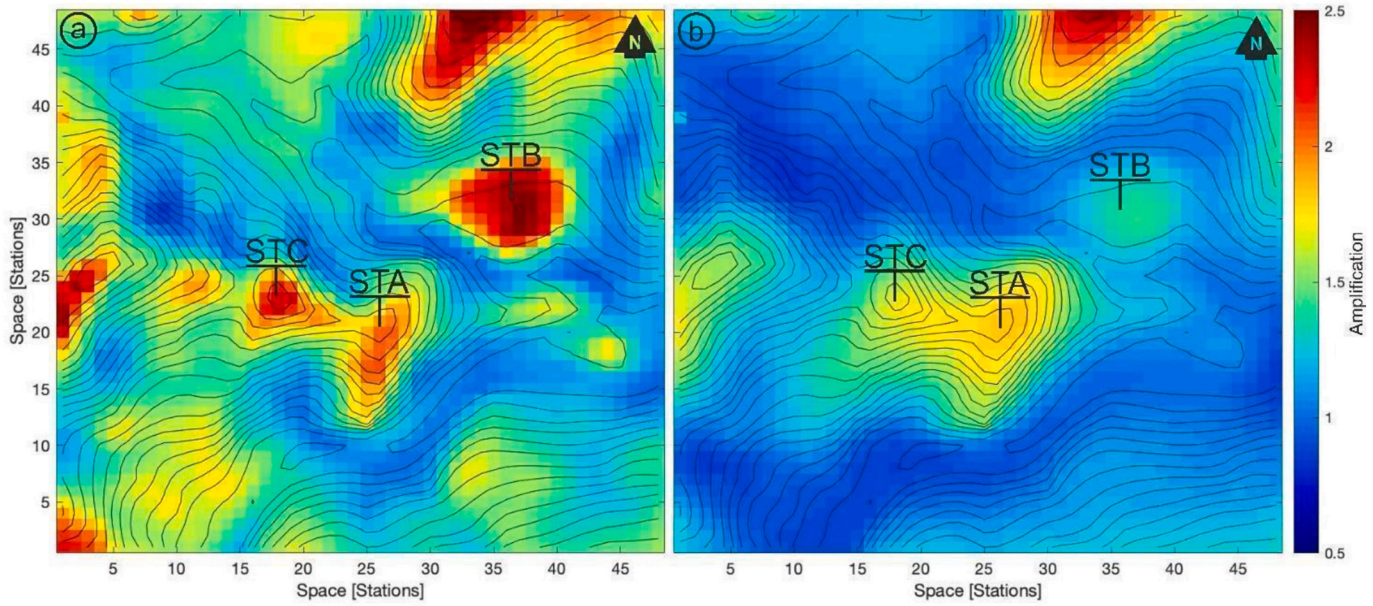

Fig. 14. Housner's amplification factors FA_H over the study case area, calculated in the period range: 0.1–0.5 s (a) and 0.5–1 s (b) from 3D simulations.

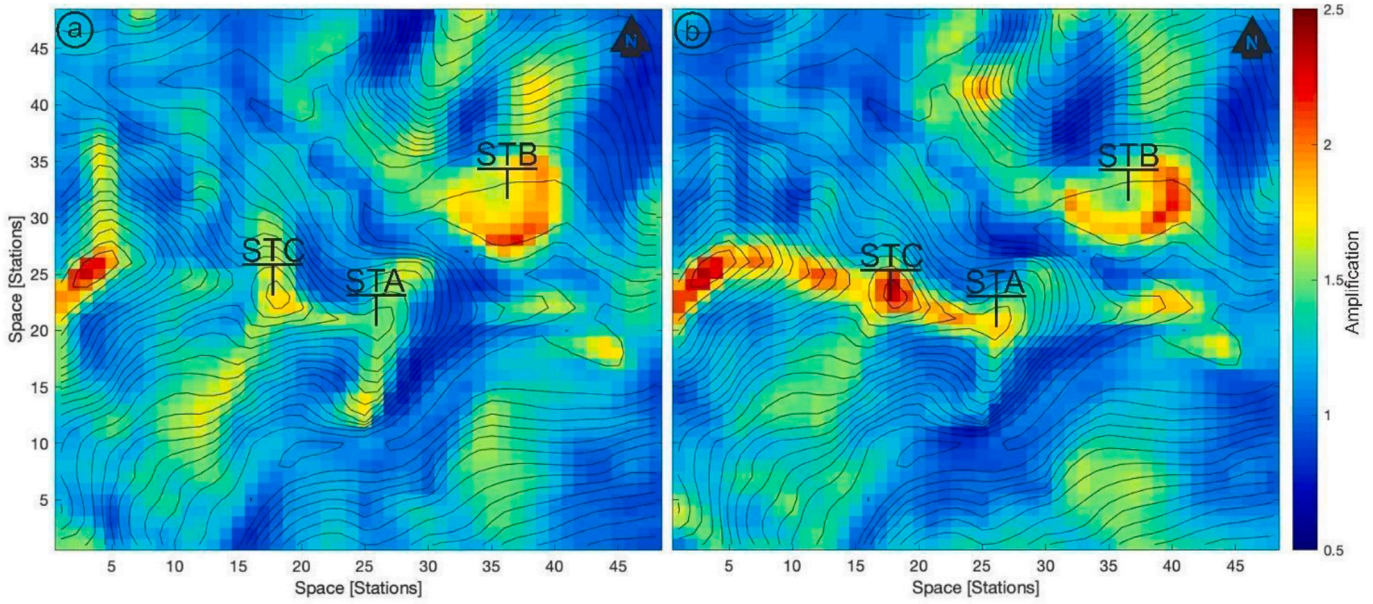

Fig. 15. The distribution of the peak values of the time-domain response function horizontal components (a) and horizontal components (b) evidences the dependence of the response of the 3D model to the polarization of the upcoming S-wave.

microzoning activities, wherever urban areas are set on or nearby complex rocky relieves especially when a weathered rocky mass level is detected. To this end, an adequate amount of geological and geophysical data must be collected to reconstruct representative 3D models of the ridges.

Author contribution

Ilaria Primofiore: Methodology, Data Curation, Software 2D and 3D, Visualization, Formal analysis, Writing - Review & Editing. **Julie Baron:** Methodology, Software 3D, Formal analysis, Visualization, Writing - Original Draft. **Peter Klin:** Conceptualization, Methodology, Data Curation, Software 3D, Formal analysis, Writing - Review & Editing, Validation, Supervision. **Giovanna Laurenzano:** Conceptualization, Methodology, Data Curation, Software 3D, Formal analysis, Writing - Review & Editing, Validation, Supervision. **Cristina Muraro:** Investigation, Resources, Writing - Original draft, Validation. **Franco Capotorti:** Investigation, Resources, Validation. **Marco Amanti:** Investigation, Resources, Supervision. **Giovanna Vessia:** Conceptualization, Methodology, Software 2D, Formal analysis, Writing - Review & Editing, Supervision, Project administration.

Funding sources

The research reported in this work was supported by INOGS and CINECA under HPC-TRES program award number 2017–22 (J. B.). I.P. received a Master thesis award protocol n. 154/2019 [UOR: D05 - Classif. III/2] from the Department of Engineering and Geology (INGEO)

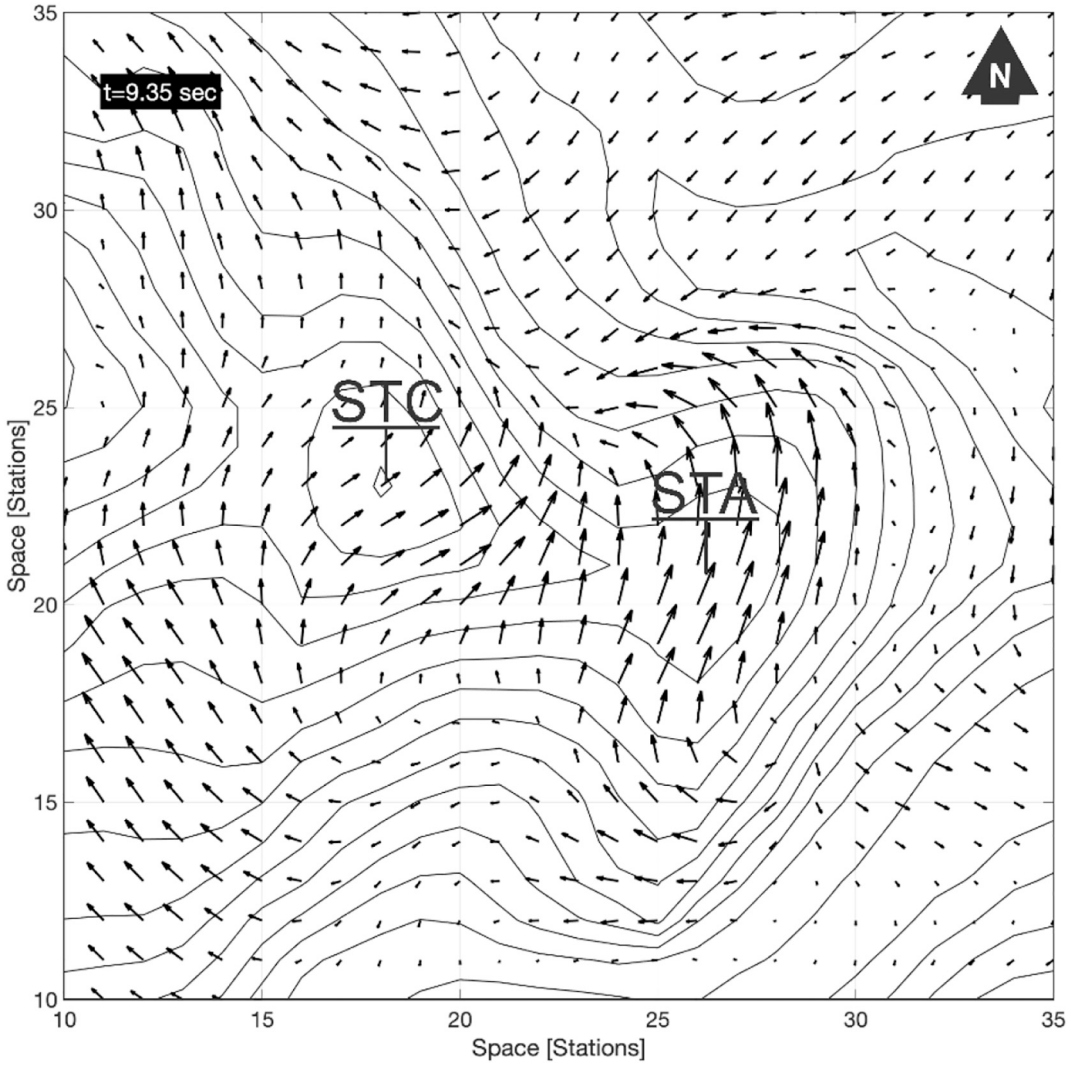

Fig. 16. Distribution of the instantaneous acceleration vectors over the surface of the 3D model on the ridge where Arquata del Tronto hamlet is located.

- "G. d'Annunzio" University for this research work.

Declaration of Competing Interest

The content of the paper does not pose any conflict of interest.

Acknowledgements

We would like to thank Luca Maria Puzzilli, Mauro Roma, Vittorio Chiessi and Fernando Ferri for their contribution in the definition of the geological and geophysical model of the study area. We acknowledge the CINECA award under the ISCRA initiative, for the availability of high performance computing resources and support. The authors are grateful to scientists from the Microzoning Center (CentroMS) for the fruitful discussions and suggestions. Signal processing and figures have been done with Matlab 2018, 9.5.0.1067069 (R2018b) Update 4, Natick, Massachusetts: The MathWorks Inc. We thank the Computational Infrastructure for Geodynamics (http://geodynamics.org) which is funded by the National Science Foundation under awards EAR-0949446 and EAR-1550901, for the availability of SPECFEM3D code. This study has been developed within the framework of the Research agreement n. 47058 on 02/07/2019 between the OGS National Institute and UdA University. Finally, the authors are grateful to the anonymous reviewers and the handling editor, for the valuable comments that highly improved the paper.

Appendix A. Geological characters

The Apennines are a North and North-East verging fold-and-thrust belt, originated by the convergence and collision between the African (Adria-Apulia) and European plates. The Central-Northern portion of this chain is a tectonic arch, bordered in the South by the E-NE verging Olevano-Antrodoco-Sibillini Mountains thrust (OASt) (Pizzi et al., 2017 and references therein). During Early Pliocene age, the OASt caused the overlapping of the Umbria-Marche basinal carbonate succession above the Latium-Abruzzi carbonate platform in the South part and above Messinian foredeep siliciclastic deposits of the Laga Basin and minor siliciclastic basins in the Northern Marche region, and above the Gran Sasso succession (Centamore et al., 1991). During Pleistocene, the activation of normal faults, mainly NW-SE or NNW-SSE oriented, affected the inner portions of the thrust belt and conditioned the present-day geological setting. Arquata del Tronto is located on the outer edge of the Central Apennines at the foot of

the OASt, in the Western outcropping area of the Messinian turbidite deposits of the Laga Formation. In this portion, this unit is also deformed by thrusts and folds (Centamore et al., 1991). The Laga Formation was firstly subdivided into three members: pre-evaporitic, evaporitic and post-evaporitic, related to the main Messinian events of the Mediterranean region. Facies analysis allowed interpreting the Laga Formation as a classical deep-sea fan turbidite succession (Milli et al., 2013 and references herein). Subsequently, the formation is subdivided into sub-members characterized by different content of arenite and pelite.

In the analysed area, four lithofacies associations of this member crop out.

The arenaceous association (LAG_{4c}) consists of arenaceous layers from thick to very thick, blended or separated by thin pelitic intercalations. The bodies have large-scale tabular and lenticular geometries, prevailing facies A1, A2, B1, B2, C1 and C2. At various heights, there are arenaceous-pelitic and subordinately pelitic-arenaceous non-mappable horizons. The succession can be ascribed to channelled deposits of an internal fan. The arenaceous-pelitic association I (LAG_{4d}) consists of alternations of arenaceous horizons in very thick layers, in facies A1, B1 and C1 and arenaceous-pelitic horizons in facies C2, C1 and D1. The A/P ratio is between 3 and 10. The surfacing unit has at least three fracture systems and is sometimes altered on the surface. The arenaceous-pelitic association II (LAG_{4b}) consists of medium to thick tabular beds with the lower portion graded and upper laminated, complete sequence of Bouma (facies C and subordinately D1 and D2), ratio A/P between 1 and 3. The pelitic-arenaceous association (LAG_{4e}) consists of thin pelitic-arenaceous layers in facies D2 and D3 with intercalated, at different heights, arenaceous-pelitic horizons consisting of medium strata, in prevalent facies C2, C1, B1 and D1. The succession is attributable to non-channelled deposits of an external fan.

Appendix B. Theoretical features of GeoModeller

GeoModeller, the package we adopt for the geological 3D modelling is, a commercial software originally developed by the French Bureau de Recherches Géologiques et Minières (BRGM) and then by the Intrepid Geophysics (http://www.geomodeller.com, last access: 27 November 2019, Calcagno et al., 2008; Guillen et al., 2004). This software allows building complex and implicit 3D geological models directly from geological observations. The interpolation method is based on the potential field theory (Lajaunie et al., 1997), so that geological interfaces (i.e. the upper or lower surfaces of the geological units) are modelled as isosurfaces of a scalar potential field defined in the 3D space. Structural data are treated as the gradient of the field. The interpolation of the field uses co-Kriging (Vessia et al., 2020a, 2020b and references therein) to take both contacts and structural data into account and generates surfaces that honour all the data together (McInerney and Guillen, 2005). The adopted approach also employs rule-based modelling to control the relationships in the stratigraphic pile (either 'onlapping' or 'erosional'), and to control fault chronology within the fault network (Chiles et al., 2007). All the details about the application of this method for building geological models can be found in Calcagno et al. (2008).

Appendix C. 2D numerical seismic response method

2D numerical analyses have been performed using the commercial code LSR2D by Stacec s.r.l. (www.stacec.com). This 2D code implements the finite element method that allows calculating stresses and deformations, under total stress conditions, induced by the 2D propagation of horizontal shear waves SH and compressional waves P from the bedrock throughout the modelled domain of soils and rocks. The code solves the general equation of the dynamic motion at each node of the finite element mesh grid:

$$M\ddot{u} + (C_e + C_b)\dot{u} + Ku = -MI_x u_{\ddot{b},x}(t) - MI_y u_{\ddot{b},y}(t) + F_{ff}(t) \quad \text{(C.1)}$$

where: M = the global mass matrix of the equation system, C_e = global damping matrix of the finite element node system; C_b = global damping matrix of the viscous dampers at the bottom of the mesh; K = global stiffness matrix of the equation system; $\ddot{u}$ = global acceleration; vector, $\dot{u}$ = global velocity vector and u = global displacement vector of the equation system; I_x = the drag global vector along horizontal direction; I_y = the drag global vector along vertical direction; $\ddot{u}_{b,x,y}$ = horizontal and vertical components of the input acceleration vector; $F_{ff}(t)$ = dynamic forces that simulate the free field conditions at the vertical boundaries of the modelled domain.

The behaviour of soils and rocks are represented by the equivalent linear model. Through this constitutive model, the shear soil response to seismic solicitations is interpreted by an equivalent viscoelastic behaviour consisting on the shear modulus G that is updated at each time step of the analysis according to the shear strain value γ induced by the input solicitation. Its decreasing values are described by a curve measured from lab tests known as cyclic degradation curve. Accordingly, to take into account the damping effects of the cyclic degradation, the damping curve D(γ) is used to update the damping values to the shear strain level. The damping curve is derived by lab tests, too. Several curves of G(γ) and D(γ) from literature are available and often used for such numerical simulations on soils according to some physical parameters. In the case of rocks, the stiffness of the materials is much higher than the soil resistance and the hypothesis of very small shear strain deformations induced by seismic shaking is considered verified, the elastic behaviour is selected. This latter consists of fixed values of G and D assumed during the input motion.

The global damping matrix, C_e, it is obtained by assembling the finite element damping values through a classical Rayleigh scheme. For each element I, the damping can be written as:

$$C_i = \alpha_{R,i} M_i + \beta_{R,i} K_i \quad \text{(C.2)}$$

where $\alpha_{R,i}$ and $\beta_{R,i}$ are the Rayleigh coefficients and M_i and K_i are the mass and stiffness matrices of each finite element, respectively.

The whole domain has been divided into triangular or quadrangular elements which maximum side dimension is decided according to the cut off frequency, that is the maximum propagated frequency f_{max}. Commonly, for near-field sites, f_{max} = 25 Hz is assigned. Then, to avoid the numerical aliasing phenomenon, the following rule has been adopting for the maximum element side dimension (Kuhlemeyer and Lysmer, 1973):

$$h = \frac{V_s}{6 \div 8\ f_{max}} \quad \text{(B.3)}$$

The input motion (see 4.1.2.) is given at the bottom of the model domain, and results, calculated in the time domain, have been reported in terms of acceleration spectral responses and the acceleration amplification function. This latter is the ratio, in the period/frequency domain, between the

output response spectrum at a point on the upper surface of the modelled domain and the input response spectrum applied at the bottom of the model, representing the bedrock line. Finally, lateral boundary conditions have been adopted to simulate the absorption of the wave associated energy by the semi-infinite domain. This type of damping edge conditions was introduced as free-field columns, corresponding to the equations:

$$F_x = -\rho V_P \left(\dot{u}_x^m + \dot{u}_x^{ff} \right) A \tag{C.4}$$

$$F_y = -\rho V_S \left(\dot{u}_y^m + \dot{u}_y^{ff} \right) A \tag{C.5}$$

where: ρ = soil mass density of the soil; V_P: P wave velocity of the soil; V_S: S wave velocity of the soil; A: the influence area of the damping node; $\dot{u}_x^m$: node velocity in x-direction; $\dot{u}_y^{ff}$: node velocity in y-direction; $\dot{u}_x^{ff}$: node velocity of the free field column in x-direction; $\dot{u}_y^{ff}$: node velocity of the free field column in the y-direction.

References

Amanti, M., Muraro, C., Roma, M., Chiessi, V., Puzzilli, L., Catalano, S., Romagnoli, G., Tortorici, G., Cavuoto, G., Albarello, D., Fantozzi, P.L., Paolucci, E., Pieruccini, P., Caprari, P., Mirabella, F., Della Seta, M., Esposito, C., Di Curzio, D., Francescone, M., Pizzi, A., Macerola, L., Nocentini, M., Tallini, M., 2020. Geological and geotechnical models definition for 3rd level seismic microzonation studies in Central Italy. Bull. Earthq. Eng. https://doi.org/10.1007/s10518-020-00843-x.

Anagnostopoulos, S.A., Kyrkos, M.T., Stathopoulos, K., 2015. Earthquake induced torsion in buildings: critical review and state of the art. Earth Struct. 8 (2), 305–377. https://doi.org/10.12989/eas.2015.8.2.305.

Barani, S., Massa, M., Lovati, S., Spallarossa, D., 2014. Effects of surface topography on ground shaking prediction: Implications for seismic hazard analysis and recommendations for seismic design. Geophys. J. Int. 197 https://doi.org/10.1093/gji/ggu095.

Burjanek, J., Faeh, D., Pischiutta, M., Rovelli, A., Calderoni, G., Bard, P.-Y., NERA-JRA1 Working Group, 2014. Site Effects at Sites with Pro-nounced Topography: Overview & Recommendations, Research Report for EU Project NERA, p. 64.

Calcagno, P., Chilès, J.P., Courrioux, G., Guillen, A., 2008. Geological modelling from field data and geological knowledge. Part I. Modelling method coupling 3D potential-field interpolation and geological rules. Phys. Earth Planet. Inter. https://doi.org/10.1016/j.pepi.2008.06.013.

Çelebi, M., 1991. Topographical and geological amplification: case studies and engineering implications. Struct. Saf. https://doi.org/10.1016/0167-4730(91)90015-2.

Centamore, E., Adamoli, L., Berti, D., Bigi, G., Bigi, S., Casnedi, R., Cantalamessa, G., Fumanti, F., Morelli, C., Micarelli, A., Ridolfi, M., Salvucci, R., 1991. Carta Geologica dei Bacini Della Laga e del Cellino e dei Rilievi Carbonatici Circostanti (Marche meridionali, Lazio nord-orientale, Abruzzo settentrionale). Studi Geol. Camerti (Vol. Spec. 1991/2).

Chiles, J.P., Aug, C., Guillen, A., Lees, T., 2007. Modelling the Geometry of Geological Units and its Uncertainty in 3D from Structural Data - the Potential-Field Method, in: Australasian Institute of Mining and Metallurgy Publication Series.

Ciancimino, A., Lanzo, G., Alleanza, G.A., Amoroso, S., Bardotti, R., Biondi, G., Cascone, E., Castelli, F., Di Giulio, A., D'Onofrio, A., Foti, S., Lentini, V., Madiai, C., Vessia, G., 2019. Dynamic characterization of fine-grained soils in Central Italy by laboratory testing. Bull. Earthq. Eng. https://doi.org/10.1007/s10518-019-00611-6.

Davis, L.L., West, L.R., 1973. Observed effects of topography on ground motion. Bull. Seismol. Soc. Am. 63 (1), 283–298.

Del Gaudio, V., Wasowski, J., 2011. Advances and problems in understanding the seismic response of potentially unstable slopes. Eng. Geol. 122, 73–83. https://doi.org/10.1016/j.enggeo.2010.09.007.

Ding, Y., Wang, G., Yang, F., 2020. Parametric investigation on the effect of near-surface soil properties on the topographic amplification of ground motions. Eng. Geol. 273 https://doi.org/10.1016/j.enggeo.2020.105687.

DISS Working Group, 2018. Database of Individual Seismogenic Sources (DISS), Version 3.2.1: A compilation of potential sources for earthquakes larger than M 5.5 in Italy and surrounding areas. Istituto Nazionale di Geofisica e Vulcanologia. http://diss.rm.ingv.it/diss/. https://doi.org/10.6092/INGV.IT-DISS3.2.1.

Galli, P., Peronace, E., Tertulliani, A., 2016. Rapporto Sugli Effetti Macrosismici del Terremoto del 24 Agosto 2016 di Amatrice in scala MCS. Rapporto Congiunto DPC, CNR-IGAG, INGV, Roma, p. 15. https://doi.org/10.5281/zenodo.161323.

Géli, L., Bard, P.-Y., Jullien, B., 1988. The effect of topography on earthquake ground motion: a review and new results. Bull. Seismol. Soc. Am. 78, 42–63.

Giallini, S., Pizzi, A., Pagliaroli, A., Moscatelli, M., Vignaroli, G., Sirianni, P., Mancini, M., Laurenzano, G., 2020. Evaluation of complex site effects through experimental methods and numerical modelling: the case history of Arquata del Tronto, Central Italy. Eng. Geol. 272, 105646 https://doi.org/10.1016/j.enggeo.2020.105646.

Gischig, V.S., Eberhardt, E., Moore, J.R., Hungr, O., 2015. On the seismic response of deep-seated rock slope instabilities - Insights from numerical modeling. Eng. Geol. 193 https://doi.org/10.1016/j.enggeo.2015.04.003.

Graziani, L., del Mese, S., Tertulliani, A., Arcoraci, L., Maramai, A., Rossi, A., 2019. Investigation on damage progression during the 2016–2017 seismic sequence in Central Italy using the European Macroseismic Scale (EMS-98). Bull. Earthq. Eng. https://doi.org/10.1007/s10518-019-00645-w.

Grünthal, G., 1998. European Macroseismic Scale 1998 (EMS-98). Cahiers du Centre Européen de Géodynamique et de Séismologie 15, Centre Européen de Géodynamique et de Séismologie, Luxembourg, 99 pp.

Guillen, A., Lane, R., Courrioux, G., Lees, T., Calcagno, P., Mclnerney, P., 2004. Constrained gravity 3D litho-inversion applied to Broken Hill. ASEG Ext. Abstr. https://doi.org/10.1071/aseg2004ab057.

He, J., Qi, S., Wang, Y., Saroglou, C., 2020. Seismic response of the Lengzhuguan slope caused by topographic and geological effects. Eng. Geol. 265, 105431. ISSN 0013-7952. https://doi.org/10.1016/j.enggeo.2019.105431.

ISPRA, 2017. Relazione Illustrativa dello Studio di Microzonazione Sismica propedeutico al Livello 3 della Macroarea 1 Arquata del Tronto e Montegallo (AP) e Allegati - Rapporto inedito per il Dipartimento della Protezione Civile, 14 novembre 2017, Roma. 46 Carte allegate. http://www.halleyegov.it/c044006/zf/index.php/trasparenza/index/index/categoria/210.

Kakhki, M.K., Peters, F.C., Mansur, W.J., SadidKhoii, A., Rezaei, S., 2020. Deciphering site response directivity in landslide-prone slopes from ambient noise spectral analysis. Eng. Geol. 269, 105542.

Klin, P., Laurenzano, G., Adelaide Romano, M., Priolo, E., Martelli, L., 2019. ER3D: a structural and geophysical 3-D model of Central Emilia-Romagna (northern Italy) for numerical simulation of earthquake ground motion. Solid Earth. https://doi.org/10.5194/se-10-931-2019.

Komatitsch, D., Tromp, J., 1999. Introduction to the spectral element method for three-dimensional seismic wave propagation. Geophys. J. Int. https://doi.org/10.1046/j.1365-246X.1999.00967.x.

Komatitsch, D., Tromp, J., 2002. Spectral-element simulations of global seismic wave propagation – I. Validation. Geophys. J. Int. https://doi.org/10.1046/j.1365-246X.2002.01653.x.

Komatitsch, D., Vilotte, J.P., 1998. The spectral element method: an efficient tool to simulate the seismic response of 2D and 3D geological structures. Bull. Seismol. Soc. Am. 88 (2), 368–392.

Kuhlemeyer, R.L., Lysmer, J., 1973. Finite element method accuracy for wave propagation problems. J. Soil Dyn. Div. 99, 421–427.

Lajaunie, C., Courrioux, G., Manuel, L., 1997. Foliation fields and 3D cartography in geology: principles of a method based on potential interpolation. Math. Geol. https://doi.org/10.1007/bf02775087.

Lanzo, G., Tommasi, P., Ausilio, E., Aversa, S., Bozzoni, F., Cairo, R., d'Onofrio, A., Durante, M.G., Foti, S., Giallini, S., Mucciacciaro, M., Pagliaroli, A., Sica, S., Silvestri, F., Vessia, G., Zimmaro, P., 2019. Reconnaissance of geotechnical aspects of the 2016 Central Italy earthquakes. Bull. Earthq. Eng. https://doi.org/10.1007/s10518-018-0350-8.

Laurenzano, G., Barnaba, C., Romano, M.A., Priolo, E., Bertoni, M., Bragato, P.L., Comelli, P., Dreossi, I., Garbin, M., 2019. The Central Italy 2016–2017 seismic sequence: site response analysis based on seismological data in the Arquata del Tronto–Montegallo municipalities. Bull. Earthq. Eng. https://doi.org/10.1007/s10518-018-0355-3.

Lee, S.J., Komatitsch, D., Huang, B.S., Tromp, J., 2009. Effects of topography on seismic-wave propagation: an example from Northern Taiwan. Bull. Seismol. Soc. Am. https://doi.org/10.1785/0120080020.

Lermo, J., Chavez-Garcia, F.J., 1993. Site Effect Evaluation Using Spectral Ratios with Only One Station. Bulletin of the Seismological Society of America 83, 1574–1594.

Lovati, S., Bakavoli, M.K.H., Massa, M., Ferretti, G., Pacor, F., Paolucci, R., Haghshenas, E., Kamalian, S., 2011. Estimation of topographical effects at Narni ridge (Central Italy): comparisons between experimental results and numerical modelling. Bull. Earthq. Eng. 9, 1987–2005. https://doi.org/10.1007/s10518-011-9315-x.

Luo, Y., Fan, X., Huang, R., Wang, Y., Yunus, A.P., Havenith, H.B., 2020. Topographic and near-surface stratigraphic amplification of the seismic response of a mountain slope revealed by field monitoring and numerical simulations. Eng. Geol. 271, 105607.

Luzi, L., Pacor, F., Lanzano, G., Felicetta, C., Puglia, R., D'Amico, M., 2019. 2016–2017 Central Italy seismic sequence: strong-motion data analysis and design earthquake selection for seismic microzonation purposes. Bull. Earthq. Eng. 1-19.

Marzorati, S., Ladina, C., Falcucci, E., Gori, S., Saroli, M., Ameri, G., Galadini, F., 2011. Site effects "on the rock": the case of Castelvecchio Subequo (L'Aquila, central Italy). Bull. Earthq. Eng. 9 (3), 841–868.

Massa, M., Barani, S., Lovati, S., 2014. Overview of topographic effects based on experimental observations: meaning, causes and possible interpretations. Geophys. J. Int. https://doi.org/10.1093/gji/ggt341.

Maufroy, E., Cruz-Atienza, V.M., Cotton, F., Gaffet, S., 2015. Frequency-scaled curvature as a proxy for topographic site-effect amplification and ground-motion variability. Bull. Seismol. Soc. Am. https://doi.org/10.1785/0120140089.

Maufroy, E., Lacroix, P., Chaljub, E., Sira, C., Grelle, G., Bonito, L., Causse, M., Cruz-Atienza, V.M., Hollender, F., Cotton, F., Bard, P.-Y., 2018. Towards rapid prediction of topographic amplification at small scales: contribution of the FSC proxy and pleiades terrain models for the 2016 Amatrice earthquake (Italy, MW 6.0). In: 16th Eur. Conf. Earthq. Eng.

McInerney, P., Guillen, A., 2005. Building 3D geological models directly from the data? A new approach applied to Broken Hill, Australia. US Geol. Survey Open File Rep. 1428, 119–130.

Milli, S., Cannata, D., Marini, M., Moscatelli, M., 2013. Facies and geometries of lower Messinian Laga Basin turbidite deposits (central Apennines, Italy). J. Mediterr. Earth Sci. Spec. Issue 179, 225.

Moczo, P., Kristek, J., Gális, M., 2014. The Finite-Difference Modelling of Earthquake Motions: Waves and Ruptures, Finite-Difference Modelling of Earthquake Motions: Waves and Ruptures. https://doi.org/10.1017/CBO9781107415324.004.

Moore, Jeffrey R., Gischig, Valentin, Burjanek, Jan, Loew, Simon, Fäh, Donat, 2011. Site Effects in Unstable Rock Slopes: Dynamic Behavior of the Randa Instability (Switzerland). Bulletin of the Seismological Society of America 101(6) (3), 3110–3116. https://doi.org/10.1785/0120110127.

Paolucci, R., 2002. Amplification of earthquake ground motion by steep topographic irregularities. Earthq. Eng. Struct. Dyn. 31, 1831–1853. https://doi.org/10.1002/eqe.192.

Paolucci, R., Faccioli, E., Maggio, F., 1999. 3D Response analysis of an instrumented hill at Matsuzaki, Japan, by a spectral method. J. Seismol. https://doi.org/10.1023/A:1009890320625.

Peter, D., Komatitsch, D., Luo, Y., Martin, R., Le Goff, N., Casarotti, E., Le Loher, P., Magnoni, F., Liu, Q., Blitz, C., Nissen-Meyer, T., Basini, P., Tromp, J., 2011. Forward and adjoint simulations of seismic wave propagation on fully unstructured hexahedral meshes. Geophys. J. Int. https://doi.org/10.1111/j.1365-246X.2011.05044.x.

Pischiutta, M., Rovelli, A., Salvini, F., Di Giulio, G., Ben-Zion, Y., 2013. Directional resonance variations across the Pernicana fault, Mt. Etna in relation to brittle deformation fields (3), Geophys–996. https://doi.org/10.1093/gji/ggt03.

Pischiutta, M., Rovelli, A., Cara, F., Di Giulio, G., Milana, G., Vassallo, M., 2015a. Amplification on topographic irregularities: the role of morphology versus the subsurface geological structure. EGUGA 12210.

Pischiutta, M., Savage, M.K., Holt, R.A., Salvini, F., 2015b. Fracture-related wavefield polarization and seismic anisotropy across the Greendale fault. Journal of Geophysical Research: Solid Earth 120 (10), 7048–7067.

Pischiutta, M., Cultrera, G., Caserta, A., Luzi, L., Rovelli, A., 2010. Topographic effects on the hill of Nocera Umbra, Central Italy. Geophys. J. Int. 182, 977–987.

Pischiutta, M., Cianfarra, P., Salvini, F., Cara, F., Vannoli, P., 2018. A systematic analysis of directional site effects at stations of the Italian seismic network to test the role of local topography. Geophys. J. Int. 214 (1), 635–650. https://doi.org/10.1093/gji/ggy133.

Pizzi, A., Di Domenica, A., Gallovič, F., Luzi, L., Puglia, R., 2017. Fault Segmentation as Constraint to the Occurrence of the Main Shocks of the 2016 Central Italy Seismic Sequence. Tectonics. https://doi.org/10.1002/2017TC004652.

Puzzilli, L.M., Ferri, F., Eulilli, V., Calcaterra, S., Gambino, P., Porfidia, B., Roma, M., Bellaveglia, S., Bistocchi, R.M., Gattoni, M., 2019. Integrated geophysical methods for the seismic site characterization of Arquata del Tronto (AP). In: Earthquake Geotechnical Engineering for Protection and Development of Environment and Constructions- Proceedings of the 7th International Conference on Earthquake Geotechnical Engineering.

Sepúlveda, S.A., Murphy, W., Jibson, R.W., Petley, D.N., 2005. Seismically induced rock slope failures resulting from topographic amplification of strong ground motions: the case of Pacoima Canyon, California. Eng. Geol. 80, 336–348.

Seriani, G., Priolo, E., 1994. Spectral element method for acoustic wave simulation in heterogeneous media. Finite Elem. Anal. Des. https://doi.org/10.1016/0168-874X(94)90076-0.

Sextos, A., De Risi, R., Pagliaroli, A., Foti, S., Passeri, F., Ausilio, E., Cairo, R., Capatti, M. C., Chiabrando, F., Chiaradonna, A., Dashti, S., De Silva, F., Dezi, F., Durante, M.G., Giallini, S., Lanzo, G., Sica, S., Simonelli, A.L., Zimmaro, P., 2018. Local site effects and incremental damage of buildings during the 2016 Central Italy Earthquake sequence. Earthquake Spectra. https://doi.org/10.1193/100317EQS194M.

SM Working Group, 2015. Guidelines for Seismic Microzonation, Conference of Regions and Autonomous Provinces of Italy – Civil Protection Department. Rome.

Spudich, P., Hellweg, M., Lee, W.H., 1996. Directional topographic site response at Tarzana observed in aftershocks of the 1994 Northridge, California, earthquake: implication for mainshock motion. Bull. Seismol. Soc. Am. 86, 193–208.

Tarquini, S., Isola, I., Favalli, M., Mazzarini, F., Bisson, M., Pareschi, M.T., Boschi, E., 2007. TINITALY/01: a new Triangular Irregular Network of Italy. Ann. Geophys. https://doi.org/10.4401/ag-4424.

Vessia, G., Parise, M., Tromba, G., 2013. A strategy to address the task of seismic microzoning in landslide-prone areas. Adv. Geosci. https://doi.org/10.5194/adgeo-35-23-2013.

Vessia, G., Pisano, L., Tromba, G., Parise, M., 2016. Seismically induced slope instability maps validated at an urban scale by site numerical simulations. Bull. Eng. Geol. Environ. https://doi.org/10.1007/s10064-016-0940-0.

Vessia, G., Di Curzio, D., Castrignanò, A., 2020a. Modeling 3D soil lithotypes variability through geostatistical data fusion of CPT parameters. Sci. Total Environ. https://doi.org/10.1016/j.scitotenv.2019.134340.

Vessia, G., Di Curzio, D., Chiaudani, A., Rusi, S., 2020b. Regional rainfall threshold maps drawn through multivariate geostatistical techniques for shallow landslide hazard zonation. Sci. Total Environ. https://doi.org/10.1016/j.scitotenv.2019.135815.

Xie, Z., Komatitsch, D., Martin, R., Matzen, R., 2014. Improved forward wave propagation and adjoint-based sensitivity kernel calculations using a numerically stable finite-element PML. Geophys. J. Int. https://doi.org/10.1093/gji/ggu219.

Zhang, Z., Fleurisson, J.-A., Pellet, F.L., 2018. A case study of site effects on seismic ground motions at Xishan Park ridge in Zigong, Sichuan, China. Eng. Geol. 243, 308–319.